

Study of Electron Identification Capability of ALICE TRD

A Dissertation for Master of Science
Department of Physics, Graduate School of Science, University of Tokyo
35-46118 Yuhei Morino

Contents

List of Figures	vii
List of Tables	ix
1 Introduction	1
1.1 Relativistic heavy ion collisions	1
1.2 Outline of this thesis	2
2 ALICE Transition Radiation Detector	3
2.1 TRD in ALICE	3
2.1.1 The setup of ALICE	3
2.1.2 Motivation of ALICE TRD	3
2.1.3 Requirement of ALICE TRD	5
2.1.4 General description of ALICE TRD	6
2.2 TRD principle	7
2.3 Detector design	9
2.3.1 Radiator	9
2.3.2 Readout chamber	9
2.3.3 Front-End electronics	11
2.3.4 Material budget	12
3 Test beam experiment	15
3.1 Test beam experiment in the past	15
3.2 Test beam experiment in 2004	16
3.2.1 Experimental setup	16
3.2.2 Real size TRD	17
4 Data analysis	21
4.1 Electron and Pion sample	21
4.2 The response of real size TRD	21
4.2.1 The reconstruction of the energy deposit	21
4.2.2 The response of the real size TRD for electron and pion samples	23
4.3 Electron Identification Capability	27
4.3.1 pion efficiency	27

4.3.2	One-dimensional likelihood method	29
4.3.3	bi-dimensional likelihood method	33
4.4	Simulation study	38
4.4.1	Simulation of the response of TRD	38
4.4.2	The effect of material budget corresponding to FEE	40
4.4.3	The effect of magnetic field	45
5	Conclusion	49
	Acknowledgment	51

List of Figures

1.1	QCD phase diagram	1
2.1	ALICE detector setup	4
2.2	Cut through the TRD geometry	6
2.3	An average number of TR photon as a function of momentum.	8
2.4	A schematic illustrations of the TRD principle	8
2.5	Microscope image. Left panel: Rohacell HF71 foam; Right panel: fibres mat . .	10
2.6	Wire geometry of the ALICE TRD chambers	10
2.7	The simulated current induced on the readout pads to a point charge deposit (a ^{55}Fe signal)	11
2.8	Basic logic components of the TRD Front-End Electronics.	12
3.1	A picture of the small prototype of TRD.	15
3.2	Pion efficiency of the small prototype of TRD as a function of momentum. . . .	16
3.3	A schematic view of the experimental setup.	17
3.4	A picture of real size TRD.	17
3.5	A picture of the readout board.	18
3.6	Event display of the TRD.	19
4.1	The correlation of response between the gas cherenkov counter and the lead-glass calorimeter at each momentum.	22
4.2	The PRF of the first layer of TRDs. The red lines are measured values and the blue line is the PRF which is obtained from fitting measured value.	24
4.3	The conceptual sketch of the way of definition of the energy deposit in this analysis.	24
4.4	Distributions of the total energy deposit in the first layer of real size TRD at 4 GeV/c.	25
4.5	The display of typical electron event and pion event. The left panel is the electron event and the right panel is the pion event.	25
4.6	The mean pulse height of electron and pion sample as a function of drift time at 4 GeV/c.	26
4.7	$\langle Q_e \rangle / \langle Q_{pi} \rangle$ at the first layer of TRDs as a function of drift region.	27

4.8	The distributions of energy deposit of the first layer of TRDs at each drift region at 4 GeV/c. The closed circles (red) indicate electron sample and the closed squares (blue) indicate pion sample.	28
4.9	The conceptual sketch of the way of electron identification.	29
4.10	The energy deposit distributions of electron and pion sample and these fitting lines at 4 GeV/c. The left panel is pion sample and the right one is electron.	30
4.11	Distributions of likelihood to be electron of pion and electron sample at 4 GeV/c. The blue line is pion sample and the red line is electron sample. The green line represents $p_{90\%}$	31
4.12	The pion efficiency as a function of the number of TRD layer which used for the calculation of likelihood ratio at 4 GeV/c.	32
4.13	The pion efficiency as a function of a beam momentum when 6 TRD layers are used.	32
4.14	The energy deposit distributions of electron and pion samples at each drift region at the first layer of TRD at 4GeV/c, and these fitting functions. The closed squares (blue) are pion samples and the closed circles (red) lines are electron samples. The smooth lines are these fitting functions.	34
4.15	L_e^k distributions of pion and electron samples by the bi-dimensional likelihood method at 4 GeV/c. The blue lines indicate pion sample and the red lines are electron samples. The green line corresponds to 90% electron efficiency.	35
4.16	The pion efficiencies by bi-dimensional likelihood method as a function of a beam momentum and the result of small prototype.	36
4.17	The pion efficiency of real size TRD and small prototype as a function of the number of TRD layer used for analysis.	37
4.18	The conceptual skethe of the way of the definition of the energy deposit.	38
4.19	The time reponse of preamplifier shaper to a point charge deposit ,which is used for TRD simulation.	39
4.20	The energy deposit distribution of pion and the simulation result at 4 GeV/c at the first layer of TRD.	40
4.21	The energy deposit distribution of electron and the simulation result at 4 GeV/c at the first layer of TRD.	41
4.22	The mean of the energy deposit of electron and pion as a function of drift time at 4 GeV/c. The left panel is electron and the right panel is pion.	41
4.23	The energy deposit distributions of the real data and the simulation at the 6, 8 and 10 GeV/c at the first layer of TRDs.	42
4.24	The event normalized energy spectrum of knockout electrons which arrived at the sixth layer of TRDs at 4 GeV/c in the case of pion.	43
4.25	The pion efficiency of the simulation and real data as a function of the number of TRD layers used for analysis at 4 GeV/c. The simulations are two case, with FEE and without FEE. When the numbers of TRD layers are 5 and 6, the results of the small are the extrapolated values.	44

4.26	A ratio of the pion efficiency of real size TRD to small prototype and that of the pion efficiency of the simulation with MCMs to the simulation without FEE as a function of the number of TRD layers.	45
4.27	The event normalized energy spectrum of knockout electrons which arrived at the sixth layer of TRDs at 4 GeV/c in the case of pion.	46
4.28	Pion efficiency of the simulation and real data as a function of the number of TRD layers used for analysis at 4 GeV/c. The simulations are two cases, under no magnetic field and magnetic field. When the numbers of TRD layers are 5 and 6, the results of the small are the extrapolated values.	47
4.29	Pion efficiency of the simulation and real data as a function of momentum. The simulation is under magnetic field.	48

List of Tables

2.1	Overview of specifications of ALICE TRD	7
2.2	The properties of the radiator materials	9
2.3	Material budget of ALICE TRD	13
4.1	The thresholds of the gas cherenkov counter and the lead-glass calorimeter for the identification of electron and pion	21
4.2	The run summary	23
4.3	The relationship between the drift region and the drift time.	26
4.4	The pion efficiencies of real size TRD.	37
4.5	The relationship between the drift time and the drift region	40
4.6	The pion efficiency of real size TRD and the simulation under magnetic field. . .	48

Chapter 1

Introduction

1.1 Relativistic heavy ion collisions

It is experimentally known that quarks and gluons are confined into hadrons and cannot exist as naked particles. This fact is called as quark confinement. Quark confinement has been a main topic of Quantum Chromo-Dynamics (QCD) which describes the strong interaction.

QCD has the remarkable nature, asymptotic freedom [1]. That is, the coupling constant of QCD becomes smaller as a transfer momentum becomes larger. At a low transfer momentum, the coupling constant of QCD is large (~ 1). This makes the perturbative treatment of QCD impossible at such region. So some effective theory have been applied for QCD at a low transfer momentum. Lattice calculation is also a powerful method for QCD.

Some theoretical calculations of QCD (effective model, QCD lattice calculation and so on) predict confined hadronic matter might undergo a phase transition into deconfinement state, QGP at critical temperature [3, 4]. The simple phase diagram of strongly interacting matter is

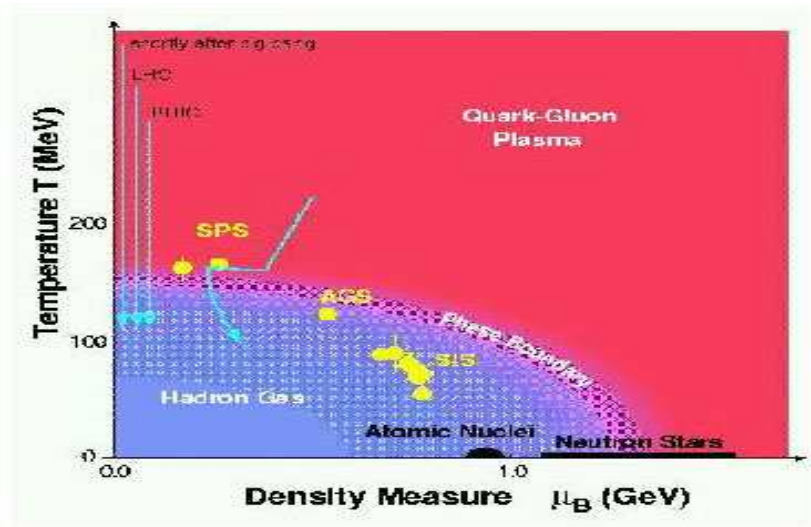


Figure 1.1: QCD phase diagram

shown in Figure 1.1.

Relativistic heavy ion collision is a powerful method to study the property of strongly interacting matter at extreme high temperature and density, specially the existence and property of QGP. The experiments at Relativistic Heavy Ion Collider (RHIC) at Brookhaven National Laboratory started in 2000. At RHIC, Au+Au collisions at $\sqrt{s_{NN}} = 200$ GeV is achieved. And various interesting results have been reported [5]. A Large Ion Collider Experiment (ALICE) will start in 2007 at Large Hadron Collider (LHC) at CERN. ALICE is optimized for Pb+Pb collision at $\sqrt{s_{NN}} = 5.5$ TeV, which is ~ 30 times larger than that of RHIC. The property of extreme hot and dense matter will be clearer through ALICE experiment.

For the study of property of extreme hot and dense matter, a measurement of various observables is necessary. Specially, measurement of quarkonia (J/ψ , Υ) is important because quarkonia signal is one of the most promising QGP signatures. The importance of the quarkonia is not only related to the physics behind the production mechanism of heavy quarks under extreme condition but also in the way how they are going to signal the formation of the QGP system. The prediction for LHC energies alternate between total suppression [10, 11] and enhancement relative to the quarkonia production in nucleon-nucleon collisions [12, 13]. Since a di-electron decay channel of the quarkonia is a good way to measure the quarkonia, the identification of electron is important at ALICE.

At the ALICE experiment, the identification of electron is the role of time projection chamber and transition radiation detector (TRD). At high momentum region (above 3 GeV/c), TRD is the main detector for electron identification. In this thesis, the capability of electron identification of ALICE TRD is studied.

1.2 Outline of this thesis

Main topic of this thesis is the capability of electron identification of ALICE Transition Radiation Detector (TRD).

In chapter 2, the properties of transition radiation and the role and design of ALICE TRD are described. In chapter 3, the setup and condition of test experiment which was held in 2004 at CERN, the response of each detector response, and the configuration of real size ALICE TRD which is used in test experiment is described. In chapter 4, the result of test experiment, specially the capability of electron identification of TRD is described. Comparison with the result of past test experiment with small prototype and consideration is also described. In chapter 5, conclusion of this thesis is summarized.

Chapter 2

ALICE Transition Radiation Detector

2.1 TRD in ALICE

2.1.1 The setup of ALICE

ALICE is an experiment at LHC optimized for heavy ion collisions at $\sqrt{s_{NN}} = 5.5$ TeV [7]. The physics goal of ALICE is to study the property of hot QGP, its dynamical evolution, hadronization, and evolution of hadronic state. It is thought that many observables need to be addressed to understand the properties of QGP accompanied by the complicated space-time evolution of the system [6]. In order to achieve the goal, ALICE is designed to measure a large set of observables.

The experimental setup of ALICE is shown in Figure 2.1. ALICE will have a central barrel, housed in the L3 magnet, covering in pseudorapidity the range $-0.9 \leq \eta \leq 0.9$ with full azimuthal coverage. The central barrel is a main part of ALICE and designed to provide excellent capability of particle tracking and particle identification. The central barrel comprises an inner tracking system of Silicon detectors (ITS), a large time projection chamber (TPC) which is the main detector for particle tracking, a transition radiation detector (TRD) which is the subject for this thesis, and a time-of-flight array (TOF) which provide hadron identification. In addition, there are two single arm detectors at close to mid-rapidity, an array of ring-imaging Cherenkov counters (HMPID) for hadron identification in the high momentum region and an array of crystals (PHOS) for photon measurements. A muon spectrometer is mounted at the pseudorapidity the range $2.5 \leq \eta \leq 4.0$ with its own dipole magnet. At more forward and backward rapidities, detectors are located to measure the multiplicity of charged particles and the time of an collision.

2.1.2 Motivation of ALICE TRD

TRDs will provide charged particle tracking and electron identification capability. Specially, TRD is the main detector for electron identification at high momentum region above 3 GeV/c. TRD will provide sufficient electron identification capability for the following measurements [8, 9].

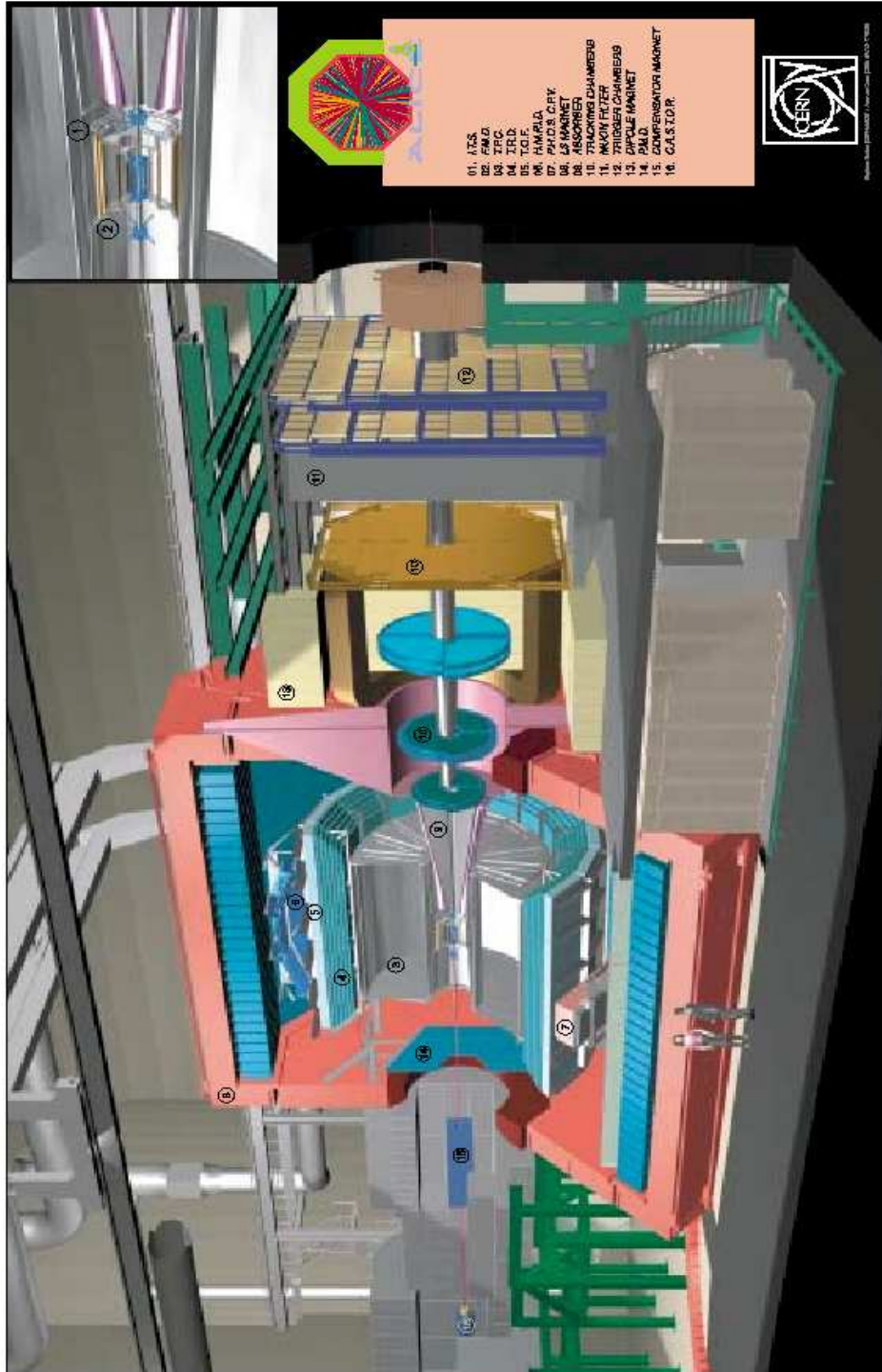


Fig.1: Layout of the ALICE detector. The Transition Radiation Detector (4) is the cyan component placed between the TPC (3) and TOF (5).

Figure 2.1: ALICE detector setup

- **Via the di-electron channel**, the production of light and heavy vector-meson. Specially, measurement of quarkonia (J/ψ , Υ) is important because quarkonia signal is one of the most promising QGP signatures [?]. And the vertex capabilities of the ITS will allow to distinguish and measure J/ψ mesons from B meson decays. A measurement of di-electron continuum between J/ψ and Υ also could be possible.
- **Via the single-electron channel**
The semi-leptonic decay of hadrons with open charm or open bottom is accessible with vertex information from ITS.
- **electron-muon coincidences**
Information from the central barrel and the forward arm gives access to correlated production of hadrons with open charm and open bottom in a rapidity range $0 \leq y \leq 4.0$

In addition, the TRD will serve as a trigger for jets with high E_t by requiring several (3 or more) high p_t tracks in one TRD module.

- **TRD as a trigger device**
The importance of the TRD as a trigger is underlined by concerning the yield of Quarkonia within the limited bandwidth of the data acquisition (DAQ). Especially, this trigger is crucial for measurement of high p_t J/ψ and Υ .

2.1.3 Requirement of ALICE TRD

To achieve the physics motivations described above, ALICE TRD is required to have the following capabilities [9].

- **Pion rejection (electron identification) capability**
ALICE TRD is required that a pion efficiency is below 1% with electron efficiency more than 90% for electron transverse momenta above 3 GeV/c. This capability of pion rejection guarantees measurement of quarkonia and the other observables described above [8].
- **Momentum resolution**
The requirement for momentum resolution is driven by the efficient and unambiguous matching to the TPC. And for the use of TRD as a trigger of high p_t track, momentum resolution of the TRD is important. ALICE TRD is required that momentum resolution to have 5% at 5 GeV under 0.4 T magnetic field.
- **The thickness of the TRD**
The radiation length of ALICE TRD must be kept to as small as possible, because additional background due to photon conversions or knockout electrons must be avoided.
- **The granularity**
High granularity is required in the bending direction by the requirement of momentum resolution and in along beam direction by requirement of capability to identify and track

electrons efficiently at high multiplicity (8000 per unit rapidity at maximum). These requirement drives the design to pads of about 6 cm^2 . TRD will achieve more than 80 % tracking efficiency.

2.1.4 General description of ALICE TRD

The requirement of capability described above led to the current design of the TRD. Figure 2.2 shows the cut thought along the beam direction of TRD. And there is also a synopsis in Table 2.1 for a quick overview.

The TRD consists of 6 individual layers for sufficient capability of electron identification. In each layer, there are 18 sectors along the azimuthal angle and 5 sectors along the beam direction as shown in Fig. 2.2. In total, there are 540 detector modules.

Each module consists of a radiator 4.8 cm thickness, a multi-wire proportional readout chamber, and the frond-end electronics for this chamber. The signal induced on the cathode pads is read out. Each chamber has 144 pads along the azimuthal angle and between 12 and 16 pads along beam direction. The pads have a typical area of $6\text{-}7 \text{ cm}^2$ and there are 1.16×10^6 readout pads in total.

The gas mixture in the readout chamber is Xe(85%) and CO_2 (15%). Each readout chamber has a drift region of 3.0 cm and an amplification region of 0.7 cm. The drift time in the drift region is $2.0 \mu\text{s}$ with the drift velocity of $1.5 \text{ cm}/\mu\text{s}$ at the electric field of $0.7 \text{ keV}/\text{cm}$. In this gas mixture, the gas gain will reach order of 5×10^3 . The details of chambers, radiators and frond-end electronics are described in Section 2.3.

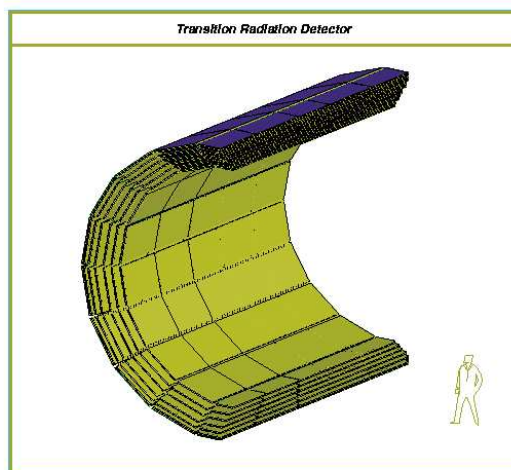


Figure 2.2: Cut thought the TRD geometry

Table 2.1: Overview of specifications of ALICE TRD

Pseudorapidity coverage	$-0.9 \leq \eta \leq 0.9$
Azimuthal coverage	2π
Radial position	$2.9 \leq r \leq 3.7$ m
Length	maximum 7.0 mm
Segments in azimuthal direction	18-fold
Segments in beam direction	5-fold
Segments in radial direction	6 layers
Total number of TRD segments	540
Largest segment size	120×159 cm ²
Detector active area	736 m ²
Detector thickness radially	$X/X_0 = 14.3$ %
Radiator	fibers+foam sandwich, 4.8 cm per layer
Number of pads in azimuthal direction	144
Number of pad rows in beam direction	12-16
Typical pad size	0.725×8.75 cm ²
Number of readout channels	1.16×10^6
Detector gas	Xe(85%) CO ₂ (15%)
Depth of drift region	3 cm
Depth of amplification region	0.7 cm
Nominal magnetic field	0.4 T
Drift field	0.7 kV/cm
Drift velocity	1.5 cm/ μ s

2.2 TRD principle

Transition Radiation (TR) was first predicted by Ginzburg and Frank in 1946 [14]. TR occurs when a relativistic charged particle passes from one medium to another medium of a different dielectric permittivity.

The TR yield depends on lorentz factor, γ of charged particle. In case of single interface between two media, TR yield is shown as Eq. 2.1.

$$W_{interface} = \frac{\alpha (\omega_1 - \omega_2)^2}{\pi (\omega_1 + \omega_2)} \gamma \quad (2.1)$$

where ω_1 and ω_2 are the plasma frequencies of the two media. Since TR yield is order of α as shown in Eq. 2.1, a radiator with an order of 100 interfaces between two media is necessary for the practical use of TR. In case of radiator with many layers, TR yield is suppressed at high γ by “interface effect” [15].

An average number of TR photons with the radiator of ALICE TRD as a function of momentum is shown in Figure 2.3, where electron is a red line, muon is a light blue, pion is a dark blue and kaon is a green. From Fig. 2.3 it is seen that More than one TR photon could

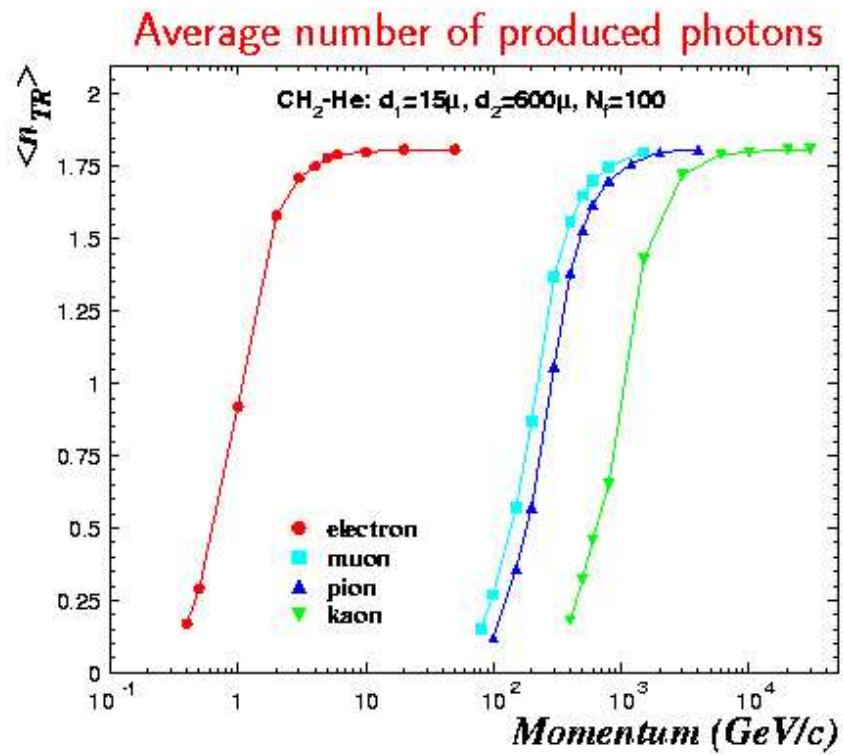


Figure 2.3: An average number of TR photon as a function of momentum.

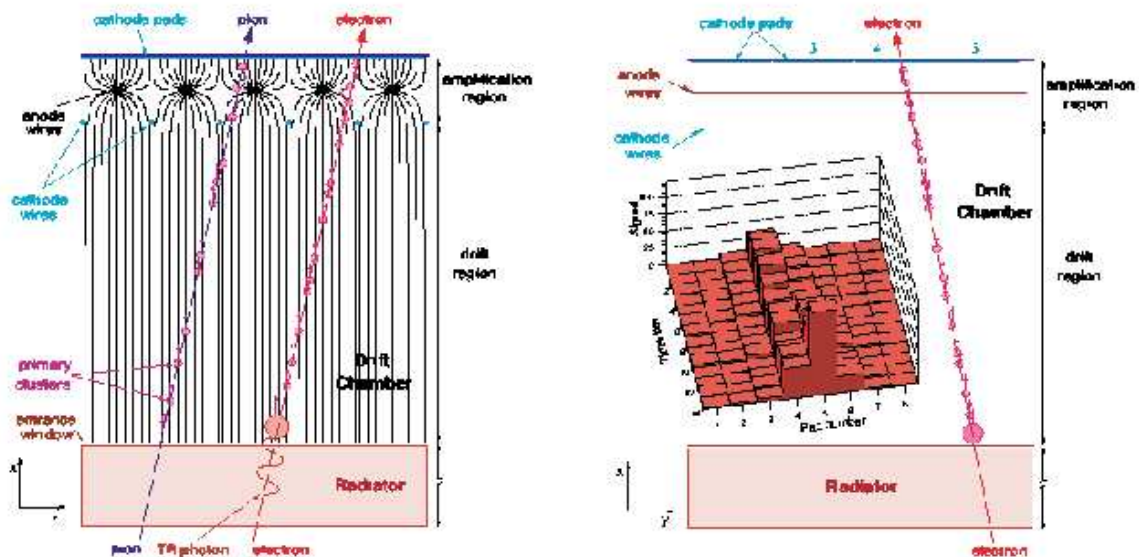


Figure 2.4: A schematic illustrations of the TRD principle

be emitted when γ excess 2000, which corresponds to about 1 GeV/c for electron and about 280 GeV/c for pion. Therefore in the momentum range from 1 GeV/c to 280 GeV/c, electron identification is possible by detection TR photon.

Figure ?? is a schematic illustrations of the TRD principle. When an electron with above 1 GeV/c momentum passes a radiator, a TR photon will be emitted parallel to the track. In case of the radiator of ALICE TRD, the energy of this TR photon is typically 10 KeV. TR photon is rapidly absorbed in the chamber which is mounted behind the radiator. So, increasing energy deposit at the entrance of the chamber is signature of an electron with emitting a TR photon. It is an essential point for electron identification by TRD.

2.3 Detector design

2.3.1 Radiator

TR photons is generated at the radiator. As described in the previous section, the probability of TR photon emission from single interface is an order of fine structure constant, so that an order of 100 boundaries have to be combined.

Due to the large areas of ALICE TRD chambers, not regular radiators but irregular radiators are chosen. In order to reduce self-absorption of emitted TR photons and keep the thickness of ALICE TRD, materials of the radiator need have low atomic number. Various materials and types (foils, foams and fibers) were systematically studied [9] and optimization was made between the thickness of TRD and TR yield. The following radiator design was chosen. The radiator consists of multi-layered media of irregular polypropylene (PP) fibers of diameter $17 \mu\text{m}$ sandwiched by the polymethacrylimid (PMI) form sheets (Rohacell HF71) of thickness of 8 mm. This PMI sheets cover upper and lower side of the PP fibers and support the entrance window of readout chamber. A carbon fiber sheets of $100 \mu\text{m}$ thickness is coated on the external sides of these PMI sheets to guarantee a flat surface of the radiator and drift electrode. The properties of these radiator materials are summarized in Table 2.2, and the images of PP fibers and PMI sheets scanned by electron microscope are shown in Figure 2.5, where left panel is PMI sheets and Right panel is PP fibers.

Table 2.2: The properties of the radiator materials

material	density[g/cm ³]	radiation length X_0 [g/cm ²]	absolute thickness[cm]	X/X_0 [*10 ⁻³]
PMI form	0.075	40.6	2*0.8	2.96
PP fiber	0.074	44.6	3.0	5.30

2.3.2 Readout chamber

The task of the readout chamber is to detect TR photons and track charged particle. For this purpose, a mixed gas with Xe (85%) and CO₂ (15%) is used for the readout chamber of ALICE

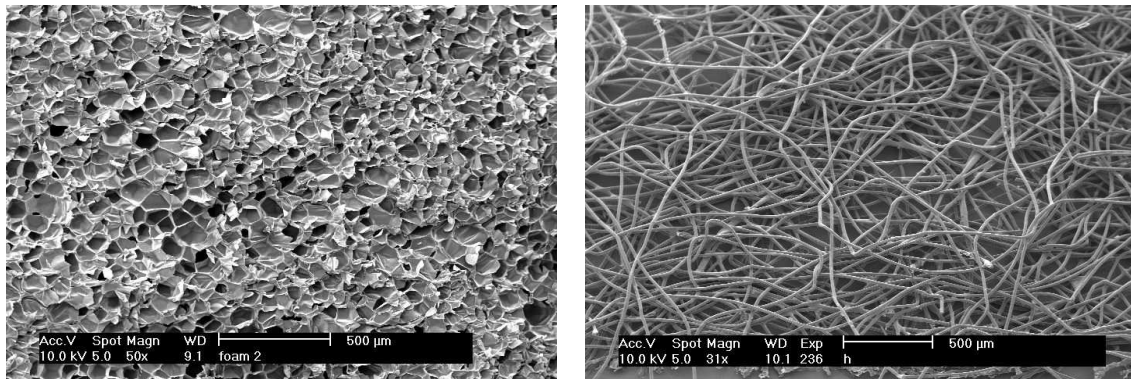


Figure 2.5: Microscope image. Left panel: Rohacell HF71 foam; Right panel: fibres mat

TRD. Xenon gas is chosen because a high probability of soft X-ray photo-absorption, and CO_2 is used as quencher.

The readout chamber have 3.0 cm drift region and 0.7 cm amplification region. Each parameter of drift region is summarized at Table 2.1. Figure 2.6 shows wire geometry at the amplification region of the readout chamber. Anode wires are biased by a positive potential (typically +1.4 kV), and cathode wires are kept at the same potential as the pad plane (ground). Wire spacing between anode wires is 5 mm and wire spacing between cathode wires is 2.5 mm.

Electrons produced in the drift volume pass through the cathode wire and start an avalanche near the anode wires, by which gas amplification reaches at the range of 10^4 order. In the process of avalanche near the anode wires, a cloud of positive ions is created and these ions moves slowly away from the anode wires to the cathod plane, including a positive signal on the pad plane. Due to the low mobility of Xe gas ions ($0.57 \text{ cm}^2/\text{Vs}$) the induced signal on the pads of a point-like primary electron cluster has a considerable tail. Figure 2.7 shows the simulated current induced on the readout pads to a point charge deposit (a ^{55}Fe signal). At track reconstruction, this tail have to be considered [16].

Readout pads are rectangular with average size $7.25 \times 87.5 \text{ mm}^2$. For good momentum resolution, the length of pads is 7.25 mm in the bending direction.

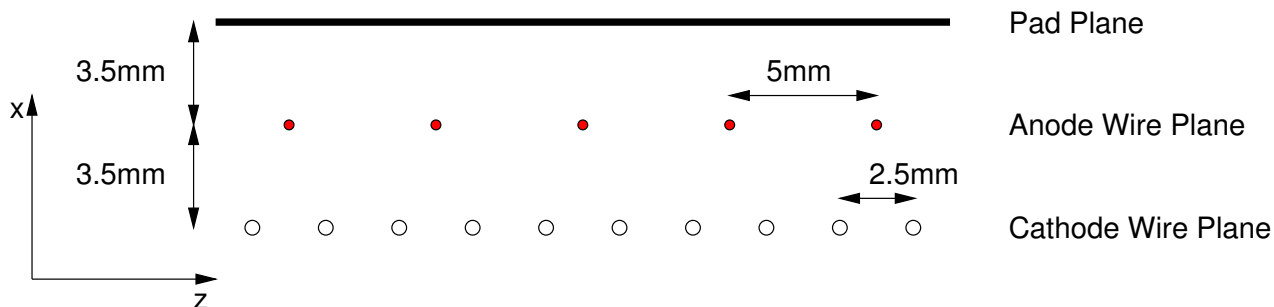


Figure 2.6: Wire geometry of the ALICE TRD chambers

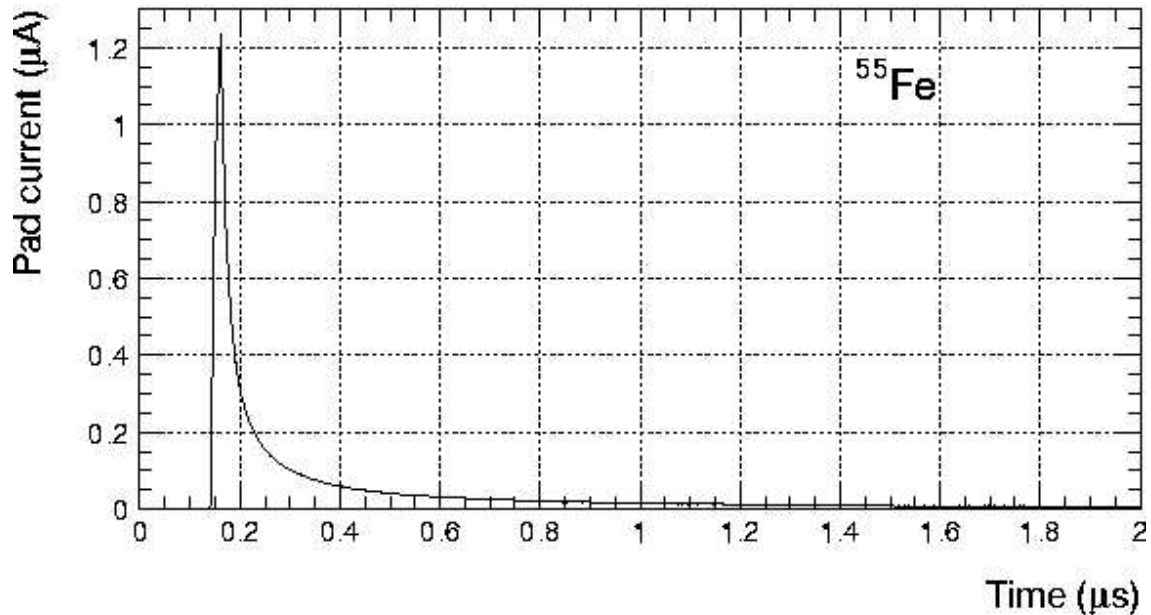


Figure 2.7: The simulated current induced on the readout pads to a point charge deposit (a ^{55}Fe signal)

2.3.3 Front-End electronics

Since the TRD will serve as a Level 1 (L1) trigger, by on-line tracking of charged particle at Front-End Electronics (FEE) with a time scale of $6\mu\text{s}$, the FEE is rather complex [16]. Figure 2.8 shows basic logic components of the TRD FEE. The FEE consist of two Application Specific Integrated Circuits (ASIC) assembled in a Multi-Chip Module (MCM). These are mounted directly on the each readout chambers.

One analog ASIC has 18 channels of charge sensitive preamplifier, shaper (PASA) and output driver. One channel has a shaping time of 120 ns at gain of 6.1 mV/fC, providing output of differential 1 V range.

One mixed analog/digital ASIC with 21 channels of 10 bits ADC, Tracklet PreProcessor (TPP) and event buffer. All channels enter one single Tracklet Processor (TP). Data digitization is done at ADC at 10 MHz frequency and at TPP data is processed (pedestal subtraction and so on) in order to prepare the information necessary for the TP during the drift time. At the end of drift time, the TP search, fit and select the tracklets. The local on-line tracking in the each TRD module is performed here.

The local trackles information of the each MCM are sent to the single Global Tracking Unit (GTU). The GTU selects high p_t track candidates form matching tracklets form different TRD layers and contributes to the Level 1 trigger.

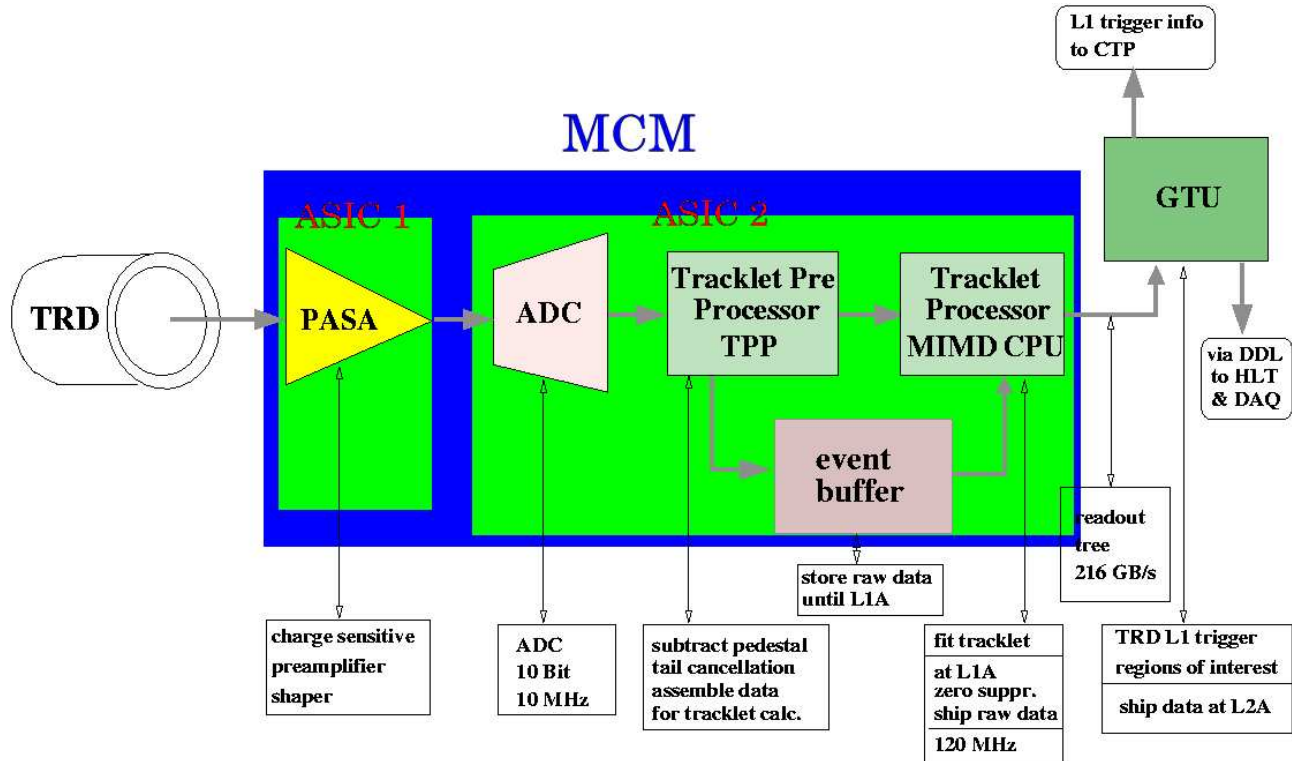


Figure 2.8: Basic logic components of the TRD Front-End Electronics.

2.3.4 Material budget

The thickness of the TRD is an important issue. The radiation thickness of all components in the active area of the TRD is summarized in Table 2.3.

Table 2.3: Material budget of ALICE TRD

Element	Material	X/X_0 [%] at $\eta = 0$
radiator	G10/Rohacell/fiber	0.93
radiator gas	air	0.02
drift electrode	metalized Mylar	0.02
drift chamber gas	Xe/CO ₂	0.24
pad plane	G10/Cu	0.13
foam backing	Rohacell	0.18
stiffening fibers	carbon fiber	0.09
readout motherboards	G10/Cu	0.44
multichip module	G10/Si/epoxy	0.14
cooling	H ₂ O/Al	0.20
1 TRD module		2.39
full TRD		14.34

Chapter 3

Test beam experiment

3.1 Test beam experiment in the past

A prototype of ALICE TRD was developed and the performance was studied [16, 17, 18, 19, 20, 21]. These measurements were performed with small prototype TRDs. The prototype were the same as ALICE TRD described in Chapter 2 except these size ($0.5 \times 0.6 \text{ m}^2$) and Front End Electronics. The electronics of the small prototypes included only charge-sensitive preamplifier/shaper (PASA), did not include a Multi-Chip Module (MCM) and readout boards (ROB). Figure 3.1 is a picture of the small prototype of TRDs.

Capability of electron identification of the small prototypes was studied [19]. Figure 3.2

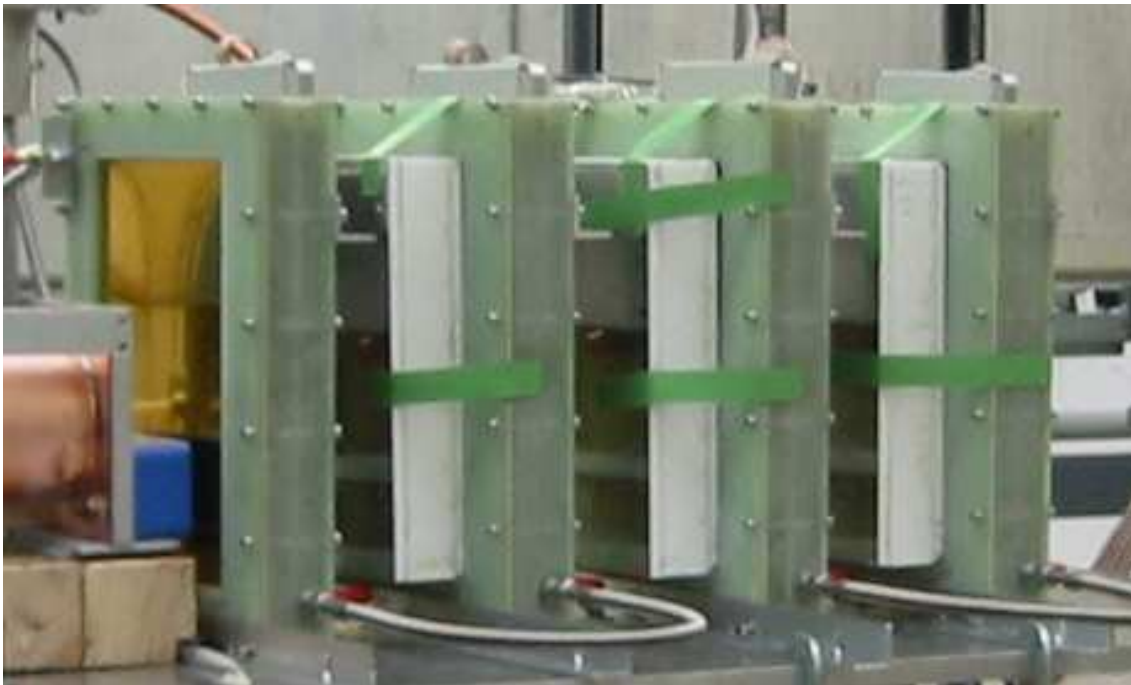


Figure 3.1: A picture of the small prototype of TRD.

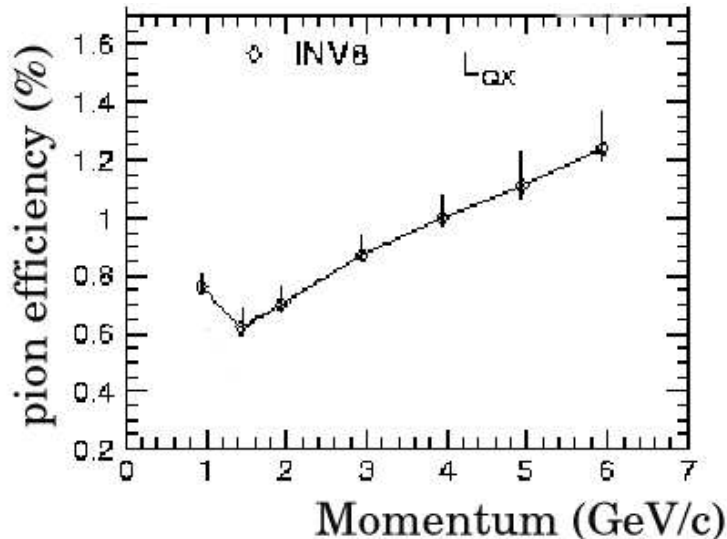


Figure 3.2: Pion efficiency of the small prototype of TRD as a function of momentum.

shows pion efficiency of the small prototype of TRD as a function of momentum. The definition of pion efficiency will be described in Chapter 4. This result is calculated from extrapolation of 4 layer TRDs to 6 layer TRDs. The requirement of the capability of electron identification is that pion efficiency is below 1 % above 3 GeV/c. The small prototypes have enough electron identification capability.

Besides the capability of electron identification, the performance of position reconstruction [17], the effect of space charge in the chambers [20], and the effect of gas contamination in the chambers [21] were studied.

3.2 Test beam experiment in 2004

3.2.1 Experimental setup

A test beam experiment with the real size ALICE TRD was performed at the T9 secondary beam line at the CERN PS accelerator. The beams consisted of electrons and pions with momenta of 1 to 10 GeV/c.

Figure 3.3 shows a schematic view of the experimental setup. Three scintillation counters (S1-S3) were used for generating the trigger signals. The sizes of the three scintillators were $5 \times 5 \text{ cm}^2$ (S1), $2 \times 2 \text{ cm}^2$ (S2) and $6 \times 6 \text{ cm}^2$ (S3), respectively. A CO_2 -filled Cherenkov counter and the lead-glass calorimeter (Pbgl) were used for separation of electron events and pion events. Since the number of electron per spill was small, Pb-glass was also used for the electron trigger in order to acquire similar sample size of electron and pion events. Four silicon strip detectors provided precise beam position information. SSD1 and SSD2 had the effective area of $32 \text{ mm} \times 32 \text{ mm}$. The strip pitch of SSD1 and SSD2 was $50 \mu\text{m}$ and the number of readout strips are 1280. And SSD3 and SSD4 had the effective area of $30.7 \text{ mm} \times 30.7 \text{ mm}$. The

strip pitch of SSD3 and SSD4 was $80\mu\text{m}$ and the number of readout strips are 768. Each SSDs consisted of two single sided silicon sensors, one is for horizontal and the other is for vertical position measurements.

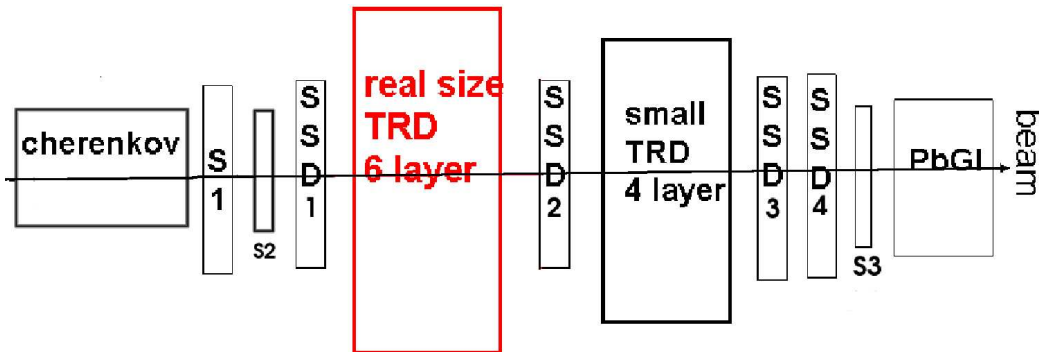


Figure 3.3: A schematic view of the experimental setup.

3.2.2 Real size TRD

Figure 3.4 is a picture of the real size ALICE TRD. This TRD consists of 6 layers and has the same size with one segment of the ALICE TRD. The size of 1, 3, 5th layers is $939 \times 1070 \times 105 \text{ mm}^2$ and the size of 2, 4, 6th layers is $981 \times 1070 \times 105 \text{ mm}^2$.

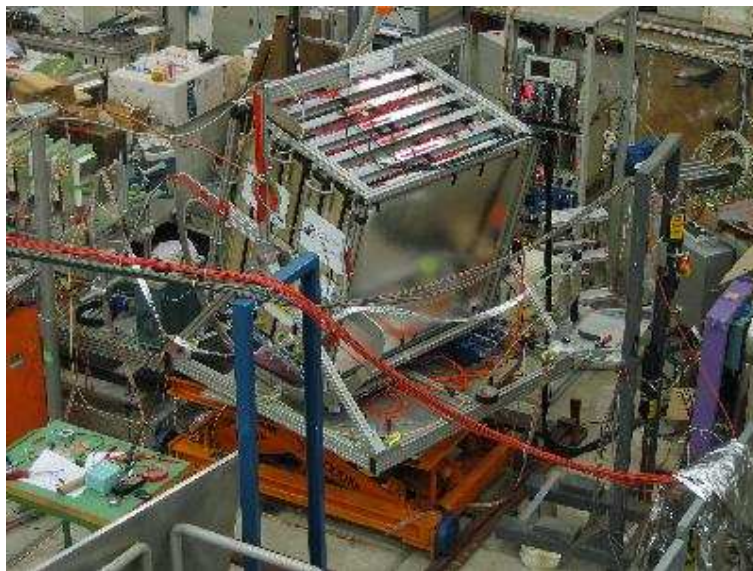


Figure 3.4: A picture of real size TRD.

In this measurement, one readout board (ROB), which was mounted on the back-end of the TRD, was used for each detector layer to read out the signals from 288 detector pads [23]. ROB consisted of 16 MCMs. As described in Chapter 2, each MCM had two chip, one is a chip for 18

channels of PASA and the other is a chip for 21 channels of ADC and digital processing. Signal digitalization (10-bit, 10 MHz sampling frequency) was performed at this board. Figure 3.5 is a picture of the ROB.

Once the data has been processed locally, it is sent through a 3-layer readout tree of MCMs, arriving via an ACEX card [24] in a readout computer. Data is converted here and travels via optical fiber into the Data Acquisition (DAQ system). The DAQ system is based on ALICE DATE v4 [25].

During this measurement, TRD was operated under atmospheric pressure and room temperature (about 20°C). Gas contaminations of oxygen and water were at the level of 40 ppm and 500 ppm, respectively. The anode voltage was 1.5 kV and the drift voltage was 1.8 kV. In this test experiment, TRD was not operated under a magnetic field. An event display of a track in the TRD is shown in Figure 3.6.



Figure 3.5: A picture of the readout board.

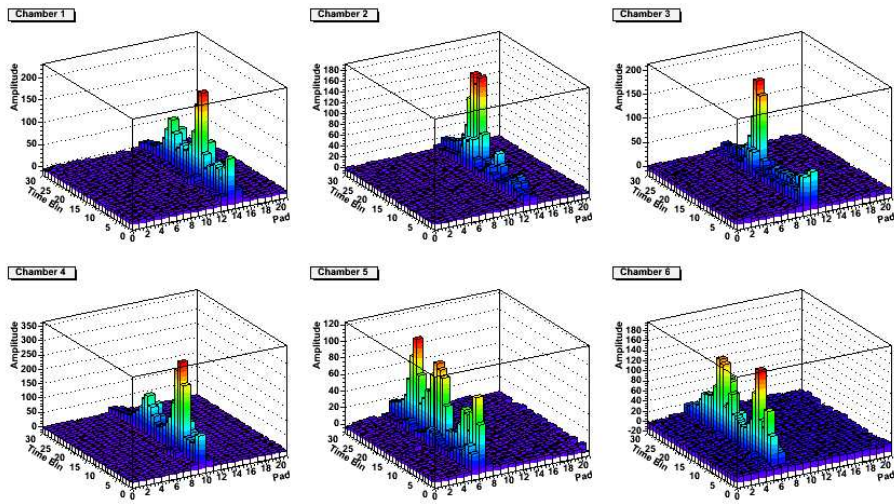


Figure 3.6: Event display of the TRD.

Chapter 4

Data analysis

4.1 Electron and Pion sample

Electron and pion events are selected using information from the gas cherenkov counter and the lead-glass calorimeter. Figure 4.1 shows the correlation of response between the gas cherenkov counter and the lead-glass calorimeter at several momentum. The thresholds of the gas cherenkov counter and the lead-glass calorimeter for the identification of electron and pion are summarized in Table. 4.1. In Fig. 4.1, black lines show the thresholds for the identification of electron and pion. The thresholds are determined so that the contamination of each sample is below 0.1%.

Only the events with single hits at least in the two 2 Silicon Strip Detectors (SSD) out of the four SSDs for the determination of the track. The numbers of analyzed events and run conditions are summarized in Table. 4.2

Table 4.1: The thresholds of the gas cherenkov counter and the lead-glass calorimeter for the identification of electron and pion

	4 GeV/c	6 GeV/c	8 GeV/c	10 GeV/c
cherenkov threshold for e (A.U.)	≥ 600	≥ 600	≥ 600	≥ 600
cherenkov threshold for pi (A.U.)	≤ 500	≤ 500	≤ 500	≤ 500
Pb-glass threshold for e (A.U.)	≥ 1550	≥ 2250	≥ 3000	≥ 3700
Pb-glass threshold for pi (A.U.)	≤ 1000	≤ 1650	≤ 2300	≤ 2600

4.2 The response of real size TRD

4.2.1 The reconstruction of the energy deposit

The induced charge of the pad plane is spread over several pads. The distribution of the induced charge over several pads is described by the pad response function (PRF). As PRF,

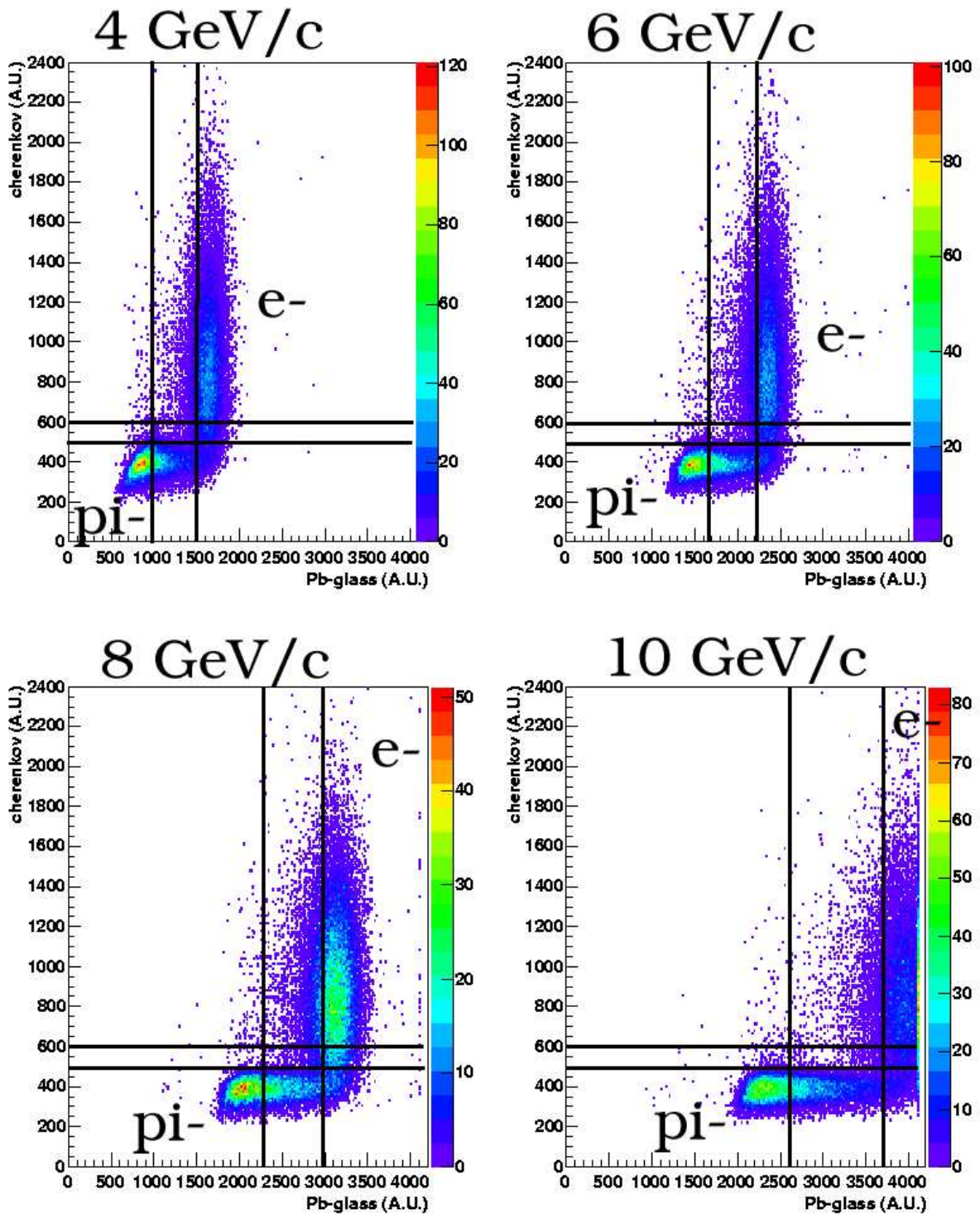


Figure 4.1: The correlation of response between the gas cherenkov counter and the lead-glass calorimeter at each momentum.

Table 4.2: The run summary

	4 GeV/c	6 GeV/c	8 GeV/c	10 GeV/c
a number of analyzed events for e	6042	6283	7980	5721
a number of analyzed events for pi	4802	4832	3904	6398
incident angle (perpendicular the anode wires) [deg]	15	15	15	15
incident angle (along the anode wires) [deg]	5	5	5	5
O ₂ contamination [ppm]	38.9	37.2	35.7	35.7
H ₂ O contamination [ppm]	450	450	500	500
CO ₂ [%]	15.1	14.9	15.1	15.1
temperature [°C]	18.1	17.6	18.0	18.1
pressure [mbar]	962	964	964	964

gauss function is chosen [26]. That is,

$$\frac{Q_i}{Q_{i-1} + Q_i + Q_{i+1}} = A \exp\left(-\frac{x^2}{2\sigma^2}\right) \quad (4.1)$$

Here, the center of the induced charge is within the i 'th pad boundary. x is the distance from the center position of the induced charge to the center of i 'th pad, and Q_i denotes the charge on the i 'th pad.

Figure 4.2 shows the PRF of the first layer of TRDs. In this figure, W is the width of pads and Q/Q_{tot} is $Q_i/(Q_{i-1} + Q_i + Q_{i+1})$. The red lines are measured values and the blue line is the PRF which is obtained from fitting measured values.

The value of σ of the PRF is typically 0.55~0.60. About 99% of the induced charge is shared at the center pad and two neighboring ones on each side. The sum of the charge of the center pad and two neighboring ones can be regarded as the total charge as a good approximation.

Figure 4.3 represents how to define the energy deposit in this analysis. The hit pad is determined using the track information obtained from SSDs, and the sum of charge of the hit pad and two neighboring ones on each side is regarded as the energy deposit. This definition is applied, because the rejection of knockout electron is crucial for the electron identification, which will be described in Section 4.4.2.

4.2.2 The response of the real size TRD for electron and pion samples

Figure 4.4 shows distributions of the total energy deposit in the first layer of real size TRD at 4 GeV/c. In Fig. 4.4, the closed squares (blue) show pion sample and the closed circles show electron sample. At 4 GeV/c, $\langle Q_e \rangle / \langle Q_{pi} \rangle = 1.67$, while $\langle Q_e \rangle / \langle Q_{pi} \rangle = 1.42$ without transition radiation, where $\langle Q_e \rangle$ denotes the mean of the total energy deposit of electrons and $\langle Q_{pi} \rangle$ denotes the pion's mean. The similar energy deposit distributions are obtained at the other TRD layers.

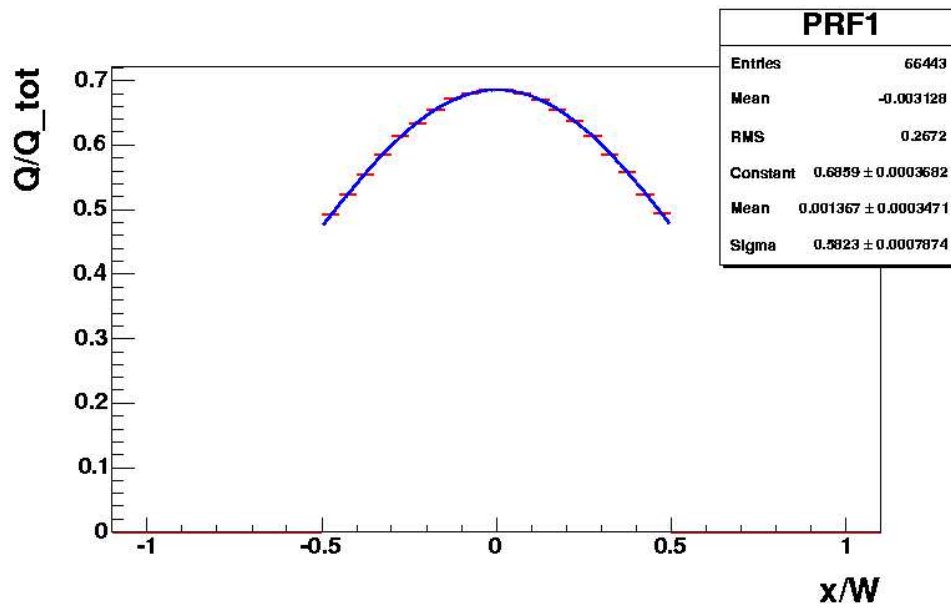


Figure 4.2: The PRF of the first layer of TRDs. The red lines are measured values and the blue line is the PRF which is obtained from fitting measured value.

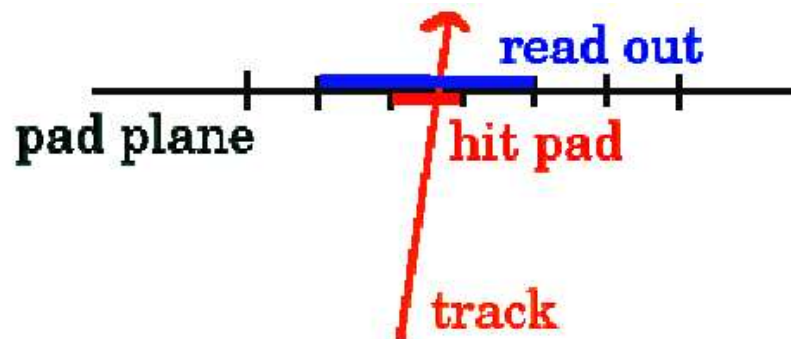


Figure 4.3: The conceptual sketche of the way of definition of the energy deposit in this analysis.

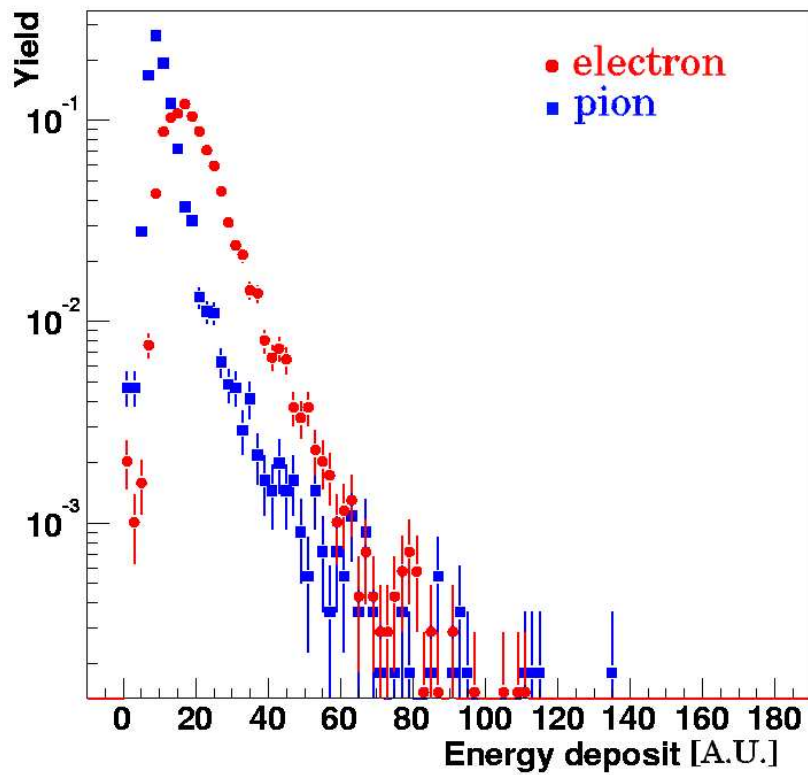


Figure 4.4: Distributions of the total energy deposit in the first layer of real size TRD at 4 GeV/c.

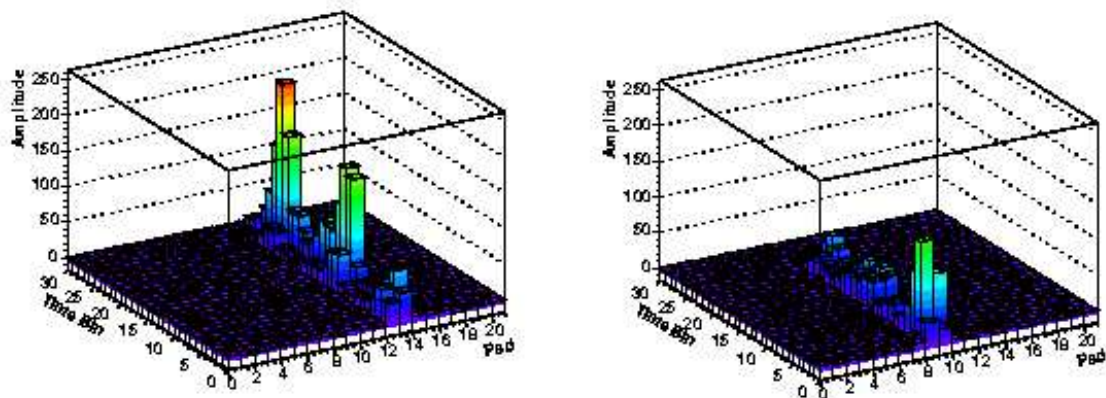


Figure 4.5: The display of typical electron event and pion event. The left panel is the electron event and the right panel is the pion event.

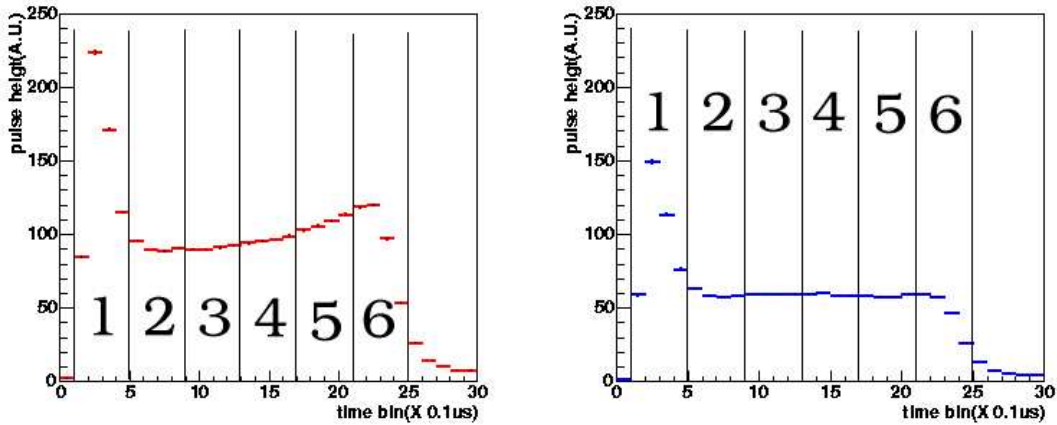


Figure 4.6: The mean pulse height of electron and pion sample as a function of drift time at 4 GeV/c.

Figure 4.5 displays typical electron and pion events. The left panel is the electron event and the right panel is the pion event. In the case of the electron event, there is a large energy deposit at the end of the drift time, which is the signature of the absorption of a TR photon at the front of the drift region.

Table 4.3: The relationship between the drift region and the drift time.

drift region	1	2	3	4	5	6
drift time (μs)	0.1-0.5	0.5-0.9	0.9-1.3	1.3-1.7	1.7-2.1	2.1-2.5

Figure 4.6 shows the mean pulse height of the electron and pion samples at the first layer of TRDs as a function of time bin (drift time) at 4 GeV/c, where the left panel is the electron sample and the right panel is the pion sample. In the right panel of Fig. 4.6, it is clearly seen that the contribution of the TR photon increases as the drift time becomes later. To evaluate this tendency qualitatively, the drift region is divided into six regions by drift time as shown in Fig. 4.6. The relationship between the drift regions and the drift time is summarized in Table 4.3. The peak at short drift time originates from the primary clusters created in the amplification region, where the ionization from both sides of the anode wires contributes to the same time interval.

Figure 4.7 shows $\langle Q_e \rangle / \langle Q_{pi} \rangle$ at the first layer of TRDs as a function of drift region at each momentum. The number of drift regions corresponds to the number in Fig. 4.6. At the last drift region (region 6), $\langle Q_e \rangle / \langle Q_{pi} \rangle$ exceeds 2.0, while $\langle Q_e \rangle / \langle Q_{pi} \rangle$ is about 1.5 at the first drift region (region 1). The drift time dependence of $\langle Q_e \rangle / \langle Q_{pi} \rangle$ is essential for electron identification.

Figure 4.8 shows the energy deposit distributions of the first layer of TRDs at each drift region at 4 GeV/c. The closed circles (red) indicate the electron sample and the closed squares (blue) indicate the pion sample. In drift regions 1 and 2, the shape of the energy deposit spectrum of the electron is almost the same as the pion's shape. The shape of the energy deposit spectrum of the electron

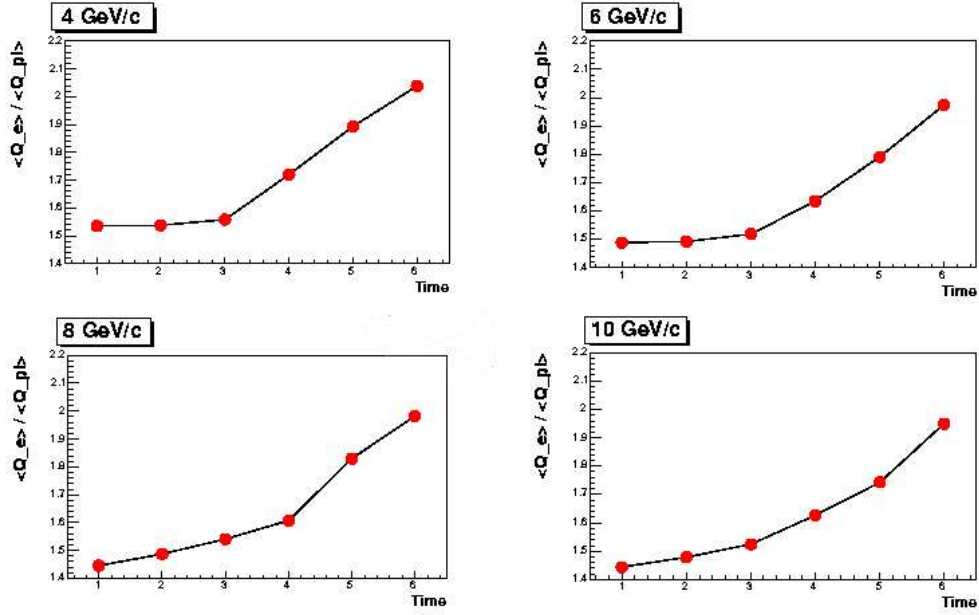


Figure 4.7: $\langle Q_e \rangle / \langle Q_{pi} \rangle$ at the first layer of TRDs as a function of drift region.

becomes very different from the pion's shape in the drift regions 5 and 6. In these region, the the energy deposit spectrum of electron have two peaks. This is because some events have the contribution from the absorption of a TR photon, and the other events do not have the contribution.

4.3 Electron Identification Capability

4.3.1 pion efficiency

Figure 4.9 is the conceptual sketch of the way of electron identification. The blue line indicates pion sample and the red line is electron sample. The green line indicates threshold for the identification of electron. The significance to be electron is calculated by a methods, in this thesis a likelihood method as described in Section 4.3.2, is used for all events. The threshold is determined by electron efficiency, and events whose significances are above this thresholds are identified electrons. Pion efficiency is used for the evaluation of the electron identification capability of TRDs. The pion efficiency is the ratio of pion events in the region by certain electron efficiency (usually 90%) to the total pion events.

Electron efficiency, E_{eff} , is defined as follows:

$$E_{eff}(p) = \frac{N(e|p \leq P_e)}{N(e|-\infty \leq P_e \leq \infty)} \quad (4.2)$$

where P_e is the significance to be electron. $N(e|p \leq P_e)$ is the number of electron events whose significance is more than a certain value, p . And $N(e|-\infty \leq P_e \leq \infty)$ is the

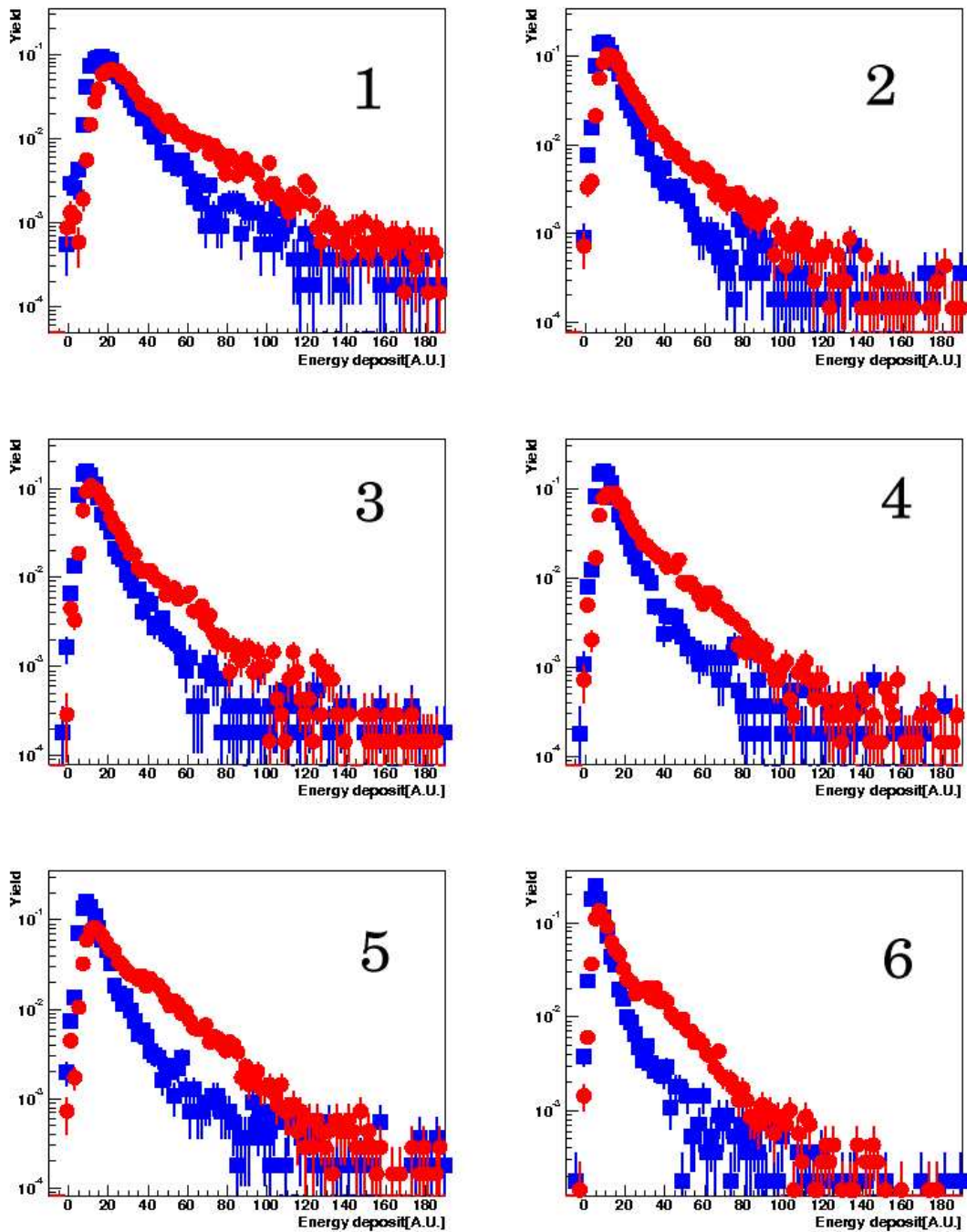


Figure 4.8: The distributions of energy deposit of the first layer of TRDs at each drift region at 4 GeV/c. The closed circles (red) indicate electron sample and the closed squares (blue) indicate pion sample.

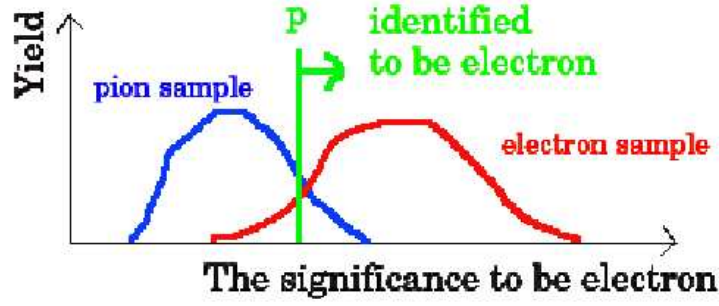


Figure 4.9: The conceptual sketch of the way of electron identification.

number of total number of analyzed electron events. In this thesis, p is determined so that $E_{eff}(p)$ becomes 90%.

Pion efficiency, $P_{\pi \rightarrow e}$, is defined as follows.

$$P_{\pi \rightarrow e} = \frac{N(\pi | p_{90\%} \leq P_e)}{N(\pi | -\infty \leq P_e \leq \infty)} \quad (4.3)$$

where $N(\pi | p_{90\%} \leq P_e)$ is the number of pion events whose significance is more than $p_{90\%}$, $N(\pi | -\infty \leq P_e \leq \infty)$ is the total number of analyzed pion events and $p_{90\%}$ satisfies the following relation:

$$0.9 = \frac{N(e | p_{90\%} \leq P_e)}{N(e | -\infty \leq P_e \leq \infty)} \quad (4.4)$$

4.3.2 One-dimensional likelihood method

One-dimensional Likelihood method is the method that likelihood ratio is used for evaluating the significance to be electron. The likelihood ratio is defined as follows.

$$L_e^k \equiv \log \frac{P_e^k}{P_\pi^k} \quad (4.5)$$

Here, P_e^k and P_π^k is determined by the energy deposit at 1st to k'th TRD layers at each event as follows.

$$P_e^k = \prod_{n=1}^k P(Q_n | e) \quad (4.6)$$

$$P_\pi^k = \prod_{n=1}^k P(Q_n | \pi) \quad (4.7)$$

Q_n is the energy deposit at n'th TRD layer. $P(Q_n | e)$ is probability that the energy deposit at n'th TRD layer becomes Q_n if the event is electron event, and Likewise, $P(Q_n | \pi)$ is probability if the event is pion event.

$P(Q_n | e)$ and $P(Q_n | \pi)$ are calculated from the function which is obtained from fitting the energy deposit distribution as shown in Fig. 4.10. The energy deposit distribution of pion

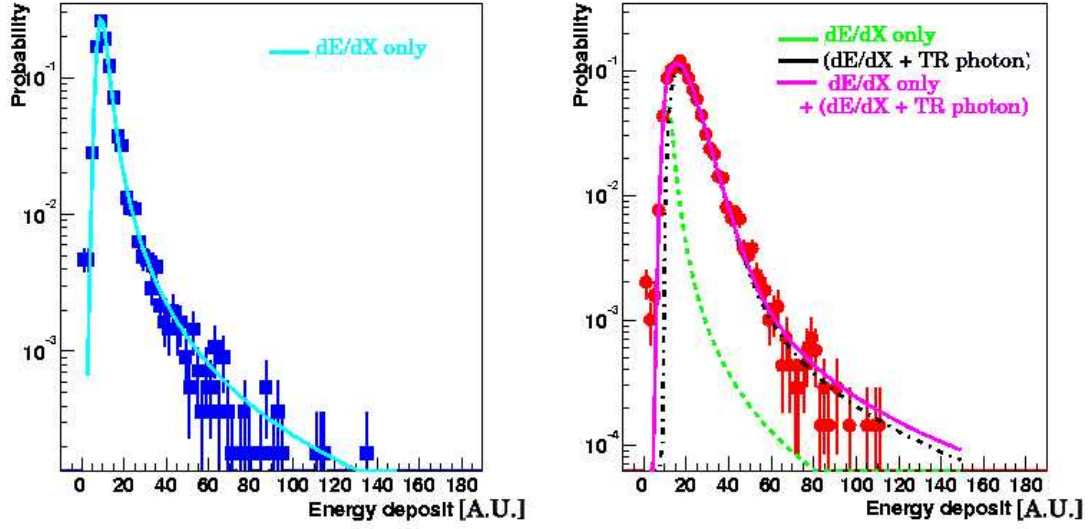


Figure 4.10: The energy deposit distributions of electron and pion sample and these fitting lines at 4 GeV/c. The left panel is pion sample and the right one is electron.

sample is fitted by convoluted Landau and Gaussian function. The energy deposit distribution of electron sample is fitted by the fuction as follows.

$$f(Q) = (1 - \alpha)g(Q) + \alpha \int_0^Q g(t) * h(Q - t)dt \quad (4.8)$$

$$h(x) = \beta x \exp(-\sqrt{\beta x}) \quad (4.9)$$

Here, $g(x)$ convoluted Landau and Gaussian is function, which represents dE/dx contribution. $h(x)$ represents the contribution of TR photon.

Based on these functions, L_e^k is calculated for pion and electron samples. Figure 4.11 shows L_e^k distribution of pion and electron samples at 4 GeV/c. In Fig. 4.11, the blue points represent pion samples and the red points represent electron samples. With increase of the number of TRD layer used for the calculation of likelihood ratio increases, clearer separation is obtained between electron and pion samples.

Figure 4.12 shows pion efficiency as a function of the number of TRD layer which used for the calculation of the likelihood ratio at 4 GeV/c. The pion efficiency reaches 1.96% when 6 TRD layers are used. Figure 4.13 shows pion efficiency as a function of a beam momentum when 6 TRD layers are used. There is the tendency which the pion efficiency becomes worse as a beam momentum increases. That is because the energy deposit of pion increases with beam momentum.

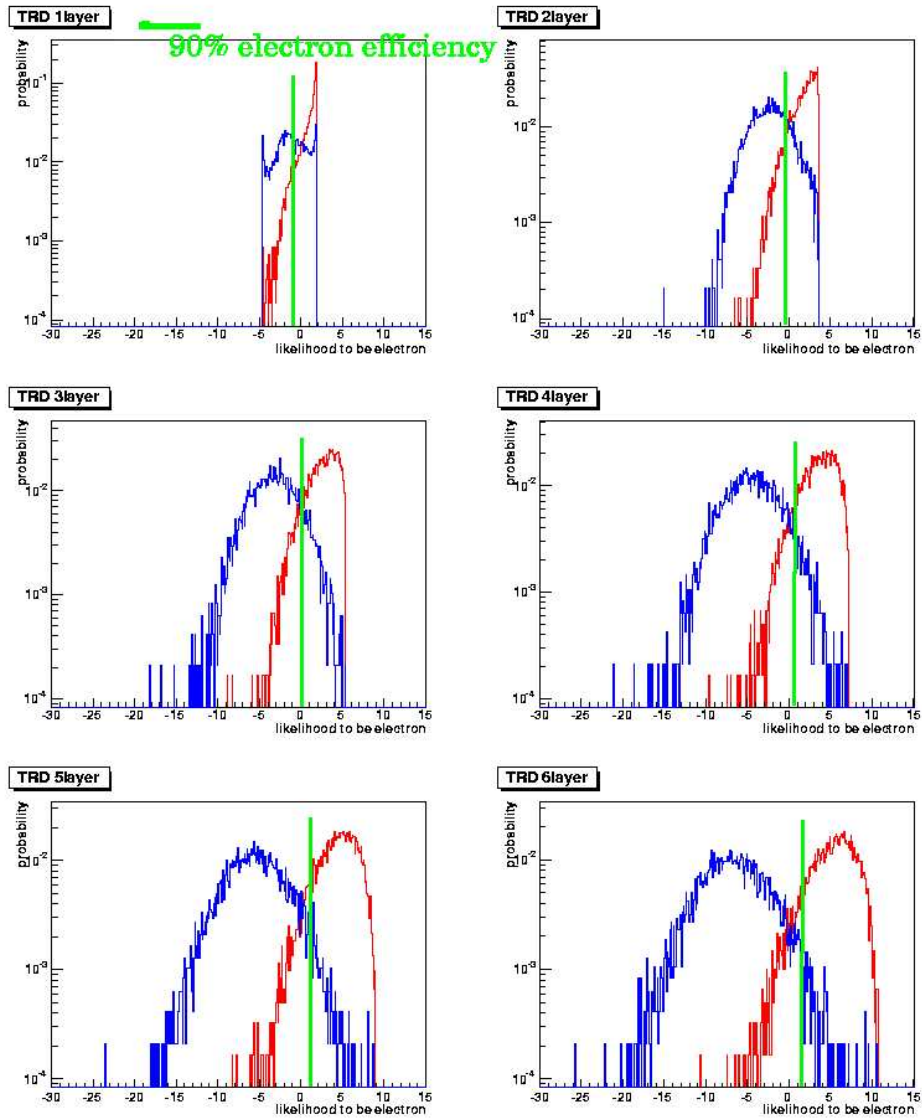


Figure 4.11: Distributions of likelihood to be electron of pion and electron sample at 4 GeV/c. The blue line is pion sample and the red line is electron sample. The green line represents $p_{90\%}$.

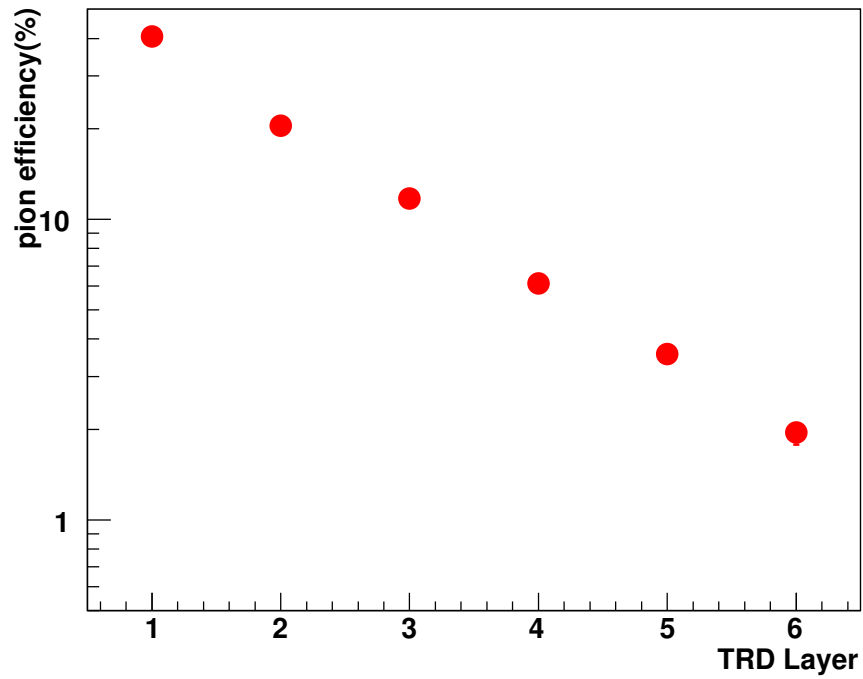


Figure 4.12: The pion efficiency as a function of the number of TRD layer which used for the calculation of likelihood ratio at 4 GeV/c.

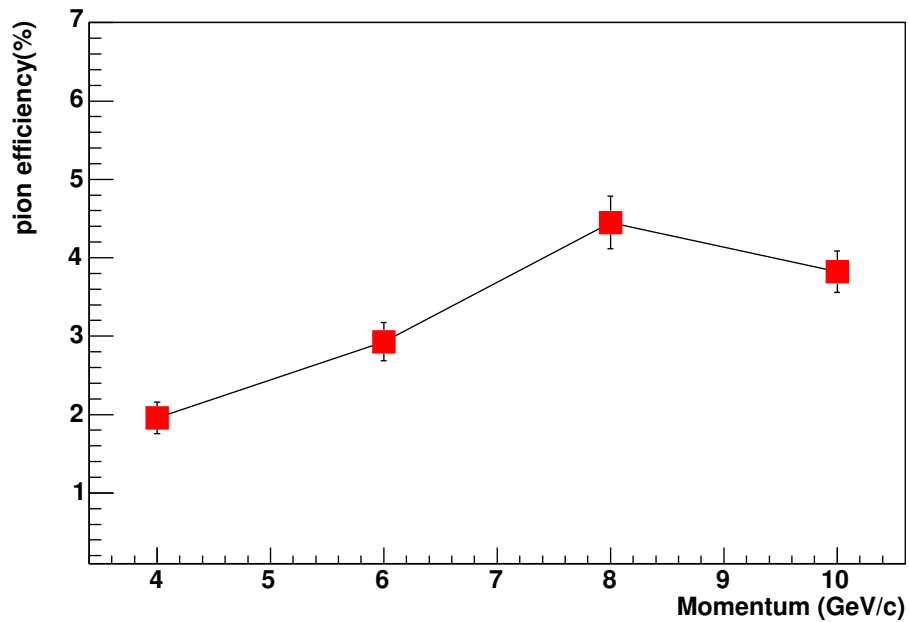


Figure 4.13: The pion efficiency as a function of a beam momentum when 6 TRD layers are used.

4.3.3 bi-dimensional likelihood method

Bi-dimensional likelihood method is used to achieve better pion efficiency than the one-dimensional likelihood method. The drift time dependence of the electron's energy loss in readout chamber differs from the drift time dependence of the pion's energy loss, as described in Section 4.2.2. By exploiting this feature, bi-dimensional likelihood could achieve better pion efficiency than one-dimensional likelihood method.

In bi-dimensional likelihood method, the likelihood ratio is used for evaluating the significance to be electron same as the one-dimensional likelihood method. The definition of likelihood ratio is given in Eq. 4.5. P_e^k and P_π^k are determined by the energy deposit at each drift region at 1st \sim k'th TRD layer as follows.

$$P_e^k = \prod_{n=1}^k \prod_{T=1}^6 P(Q_n^T|e) \quad (4.10)$$

$$P_\pi^k = \prod_{n=1}^k \prod_{T=1}^6 P(Q_n^T|\pi) \quad (4.11)$$

Here, T is the number of the drift region as defined in Section 4.2.2. Q_n^T is the energy deposit at the drift region T at n'th TRD layer. $P(Q_n^T|e)$ is probability that the energy deposit at the drift region T at n'th TRD layer becomes Q_n^T if the event is electron event. $P(Q_n^T|\pi)$ is probability in the case of pion. By calculating $P(Q_n^T|e)$ and $P(Q_n^T|\pi)$ at each drift region, the drift time dependence of the energy loss between electron and pion could be exploited.

Figure 4.14 shows the energy deposit distributions of electron and pion at each drift region at the first layer of TRD at 4GeV/c, and these fitting functions. In the figure, the number of each panel represents the drift region. The closed squares (blue) are pion samples and the closed circles (red) are electron samples. The smooth lines are these fitting functions. These fitting functions are the same as the functions used for one-dimensional likelihood method. The calculations of $P(Q_n^T|e)$ and $P(Q_n^T|\pi)$ are done based on these fitting functions.

Figure 4.15 shows L_e^k distributions of pion and electron samples by bi-dimensional likelihood method at 4 GeV/c. In this figure, the blue lines indicate pion samples and the red lines are electron samples. The green line corresponds to 90% electron efficiency. Using 6 TRD layers, the pion efficiency achieve 1.35% at 4 GeV/c. This result is better than the result of one-dimensional likelihood method, 1.96%.

Figure 4.16 shows the pion efficiency by bi-dimensional likelihood method as a function of a beam momentum and the result of the beam test at 2002 with small prototype. In the figure, the closed squares show the result of the real size TRD and the closed circles the result of small prototype. The result of small prototype is from T.Gunji's master thesis. The result of small prototype is obtained by extrapolation of the result of 4 layer small prototype to 6 layers.

The pion efficiency of the real size TRD is higher than that of small prototype. At 4 GeV/c and 5 GeV/c, the pion efficiency of small prototype is within the requirement of ALICE TRD, that is below 1% at 90% electron efficiency, while the pion efficiency of real size TRD does not fulfill the requirement.

Figure 4.17 shows the pion efficiency of the real size TRD and small prototype as a function of the number of TRD layer used for analysis. In this figure, the closed circles (red) show the

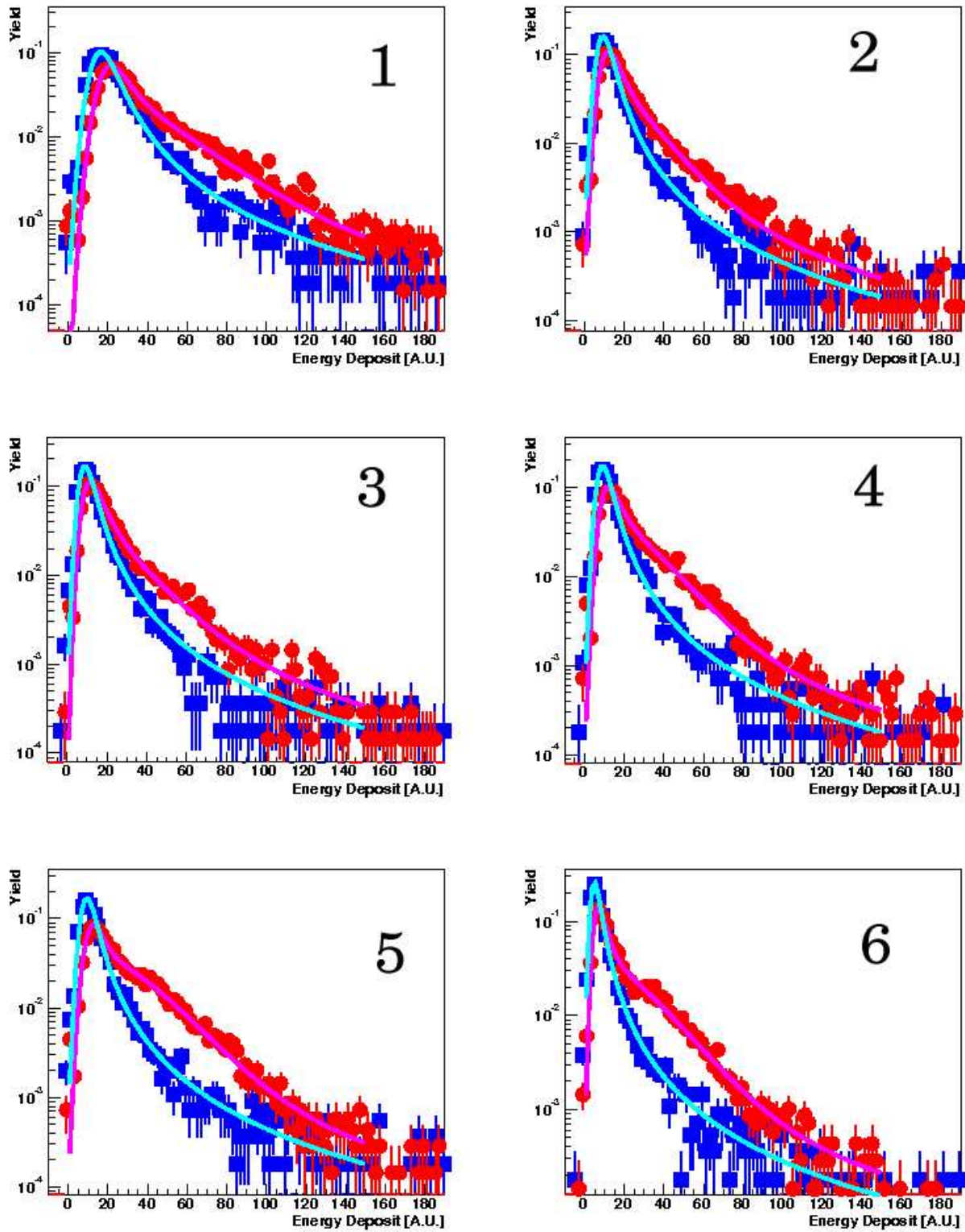


Figure 4.14: The energy deposit distributions of electron and pion samples at each drift region at the first layer of TRD at $4\text{GeV}/c$, and these fitting functions. The closed squares (blue) are pion samples and the closed circles (red) lines are electron samples. The smooth lines are these fitting functions.

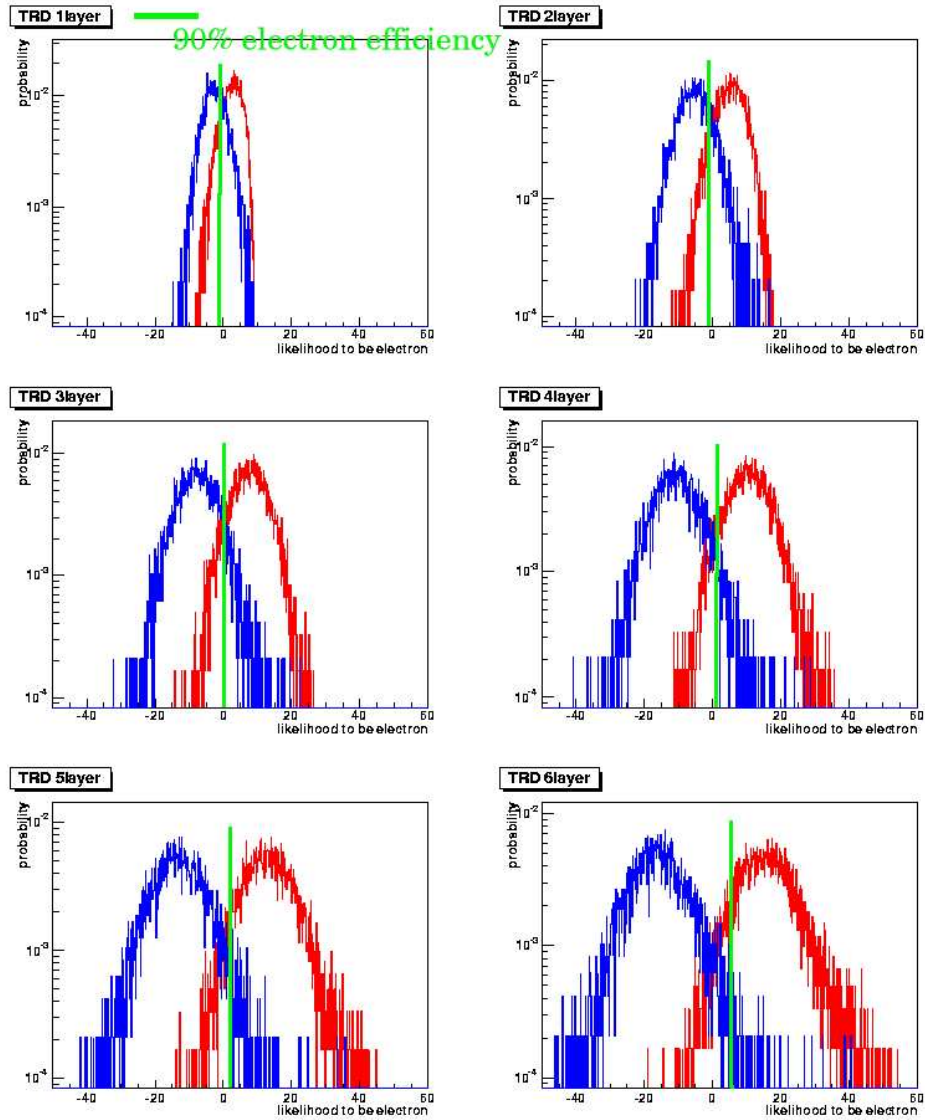


Figure 4.15: L_e^k distributions of pion and electron samples by the bi-dimensional likelihood method at 4 GeV/c. The blue lines indicate pion sample and the red lines are electron samples. The green line corresponds to 90% electron efficiency.

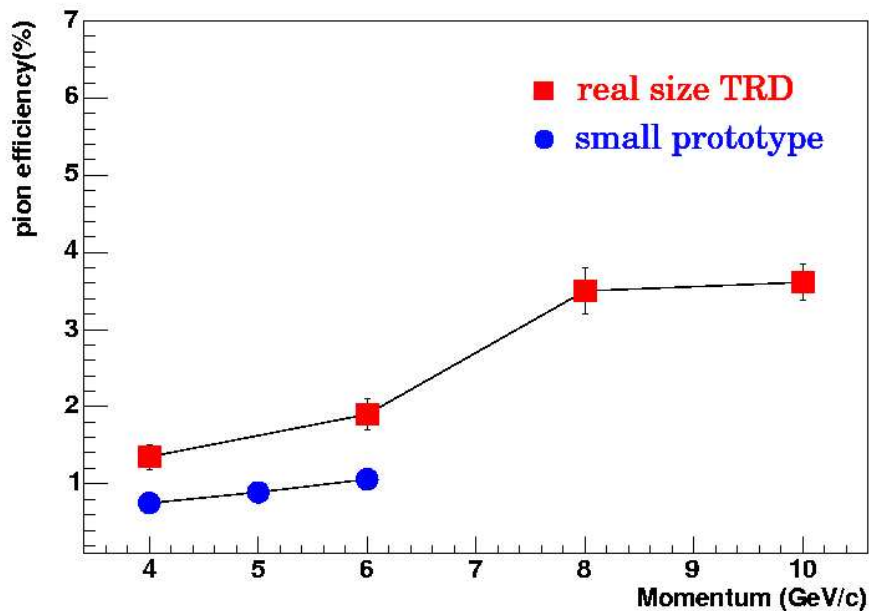


Figure 4.16: The pion efficiencies by bi-dimensional likelihood method as a function of a beam momentum and the result of small prototype.

results of the real size TRD, the closed triangles (blue) show the results of small prototype, and the reverse triangles (green) show the extrapolations of the result of the result of small prototype.

It is seen from Fig 4.17 that the pion efficiency of small prototype is slightly better than the real size TRD up to 4 layers, and the extrapolation value of the result of small prototype is much better than real size TRD. This is considered to be caused by the effect of knockout electrons. Since FEE ($X/X_0 = 0.6\%$), which is consisted of MCMs and ROB, was installed on the back of the real size TRD, but was not on the back of the small prototype, the real size TRD has larger material budget than small prototype. Due to larger material budget, the amount of knockout electrons should increase in the case of the real size TRD. Knockout electrons with large enough energy can run through the readout chamber and reach the next chamber. Consequently, the response of each TRD layer may have correlations. This is considered to be the reason that the extrapolation value of the result of the small prototype much better than real size TRD. Some results of simulation study are shown in the next section to confirm this consideration.

The pion efficiencies at each momentum by likelihood and bi-dimensional method is summarized in Table 4.4

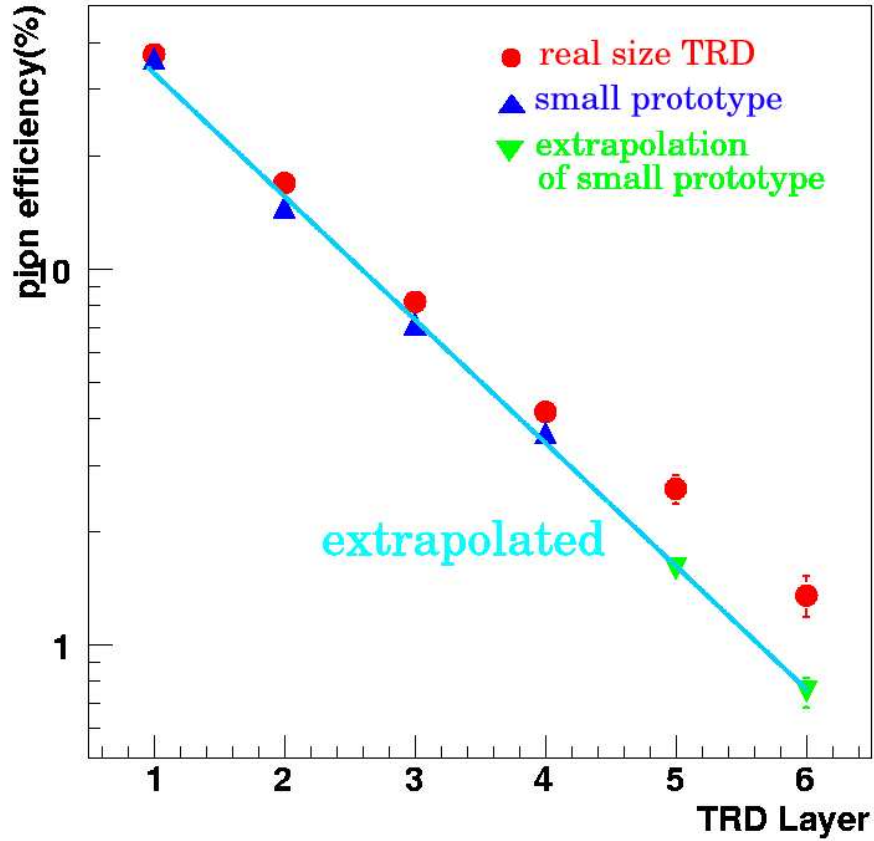


Figure 4.17: The pion efficiency of real size TRD and small prototype as a function of the number of TRD layer used for analysis.

Table 4.4: The pion efficiencies of real size TRD.

Momenta (GeV/c)	4	6	8	10
pion efficiency (one-dimensional likelihood)	1.96	2.93	4.45	3.82
pion efficiency (bi-dimensional likelihood)	1.35	1.90	3.50	3.61

4.4 Simulation study

4.4.1 Simulation of the response of TRD

Simulation is done to study the effect of knockout electrons on the capability of electron identification of the TRD. GEANT 4 [27] is used for this simulation. Simulation of TRD is prepared the almost same geometry as real size TRD and six identical TRD layer.

Physical processes (dE/dx , transition radiation and so on) are dealt with GEANT 4, and the response of TRD's readout electronics is based on the algorithm of AliRoot [28], which is the simulation toolkit for ALICE.

The first step is the calculation of energy deposit of a parent track. Here, the parent track represents a beam track. Energy deposit is defined as Eq. 4.12 and Figure 4.18. Fig 4.18 is the conceptual skethe of how to define of the energy deposit. The energy deposit in the sensitive region in Fig. 4.18 is regarded as the energy deposit in the readout chamber of TRDs.

$$\frac{dE}{dz}(z) = \int_{X_p(z)-1.5W}^{X_p(z)+1.5W} dx \int_{-l/2}^{l/2} dy \left(\frac{dE}{dz}(z) \right)_{xy} \quad (4.12)$$

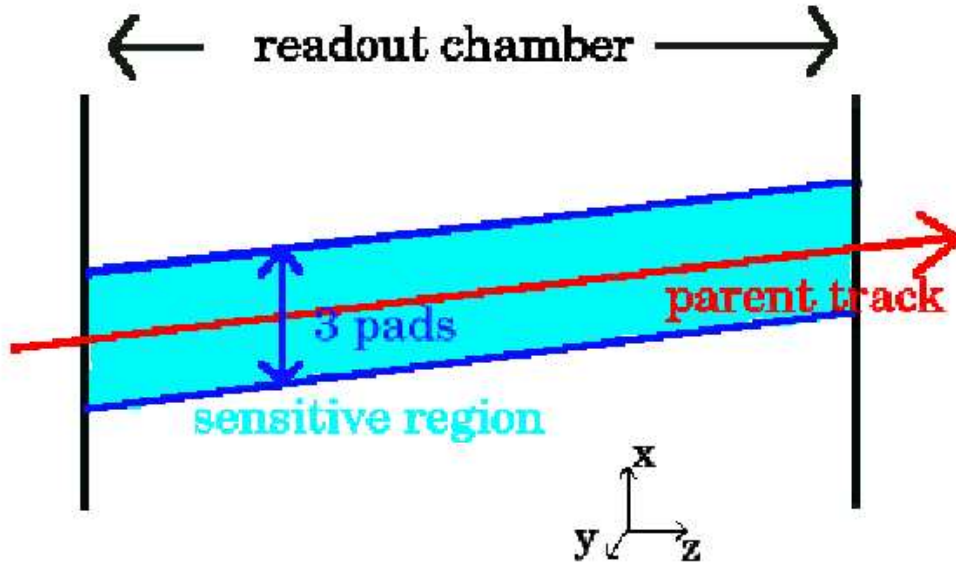


Figure 4.18: The conceptual skethe of the way of the definition of the energy deposit.

The coordinate system is defined in Fig 4.18. In Eq. 4.12, $X_p(z)$ is X position of the parent track. And W is the pad width, 6.5 mm and l is the pad length 7.5 cm. $dE/dz(z)$ represents the energy deposit at z . That is, the energy deposits are integrated over the sensitive region. The sensitive region corresponds to the way of reconstruction energy deposit in TRD analysis, as described in Section 4.2.1. There, 3 pads are used for reconstruction energy deposit.

Second step is the generation of signal of TRDs. The drift time of the enegy deposit is decided by the position of the enegy deposit and the drift velocity, which is fixed the value

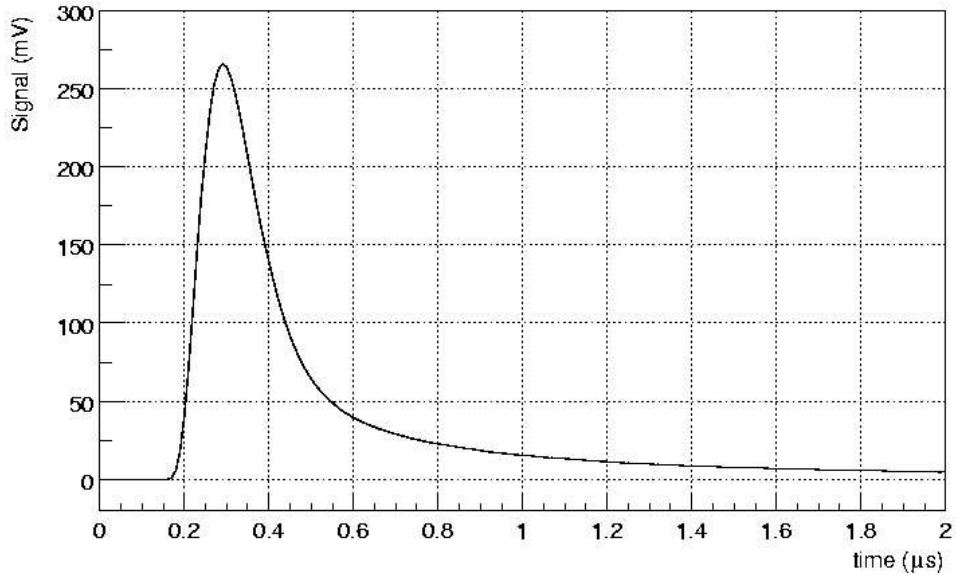


Figure 4.19: The time reponse of preamplifier shaper to a point charge deposit ,which is used for TRD simulation.

1.65 cm/ μ s. Figure 4.19 shows the time reponse of preamplifier shaper (PASA) to a point charge deposit (a ^{55}Fe signal), which is used for TRD simulation. The component of each time bin is decided, based on the response of PASA, the drift time of the energy deposit , and the value of energy deposit,

This simulation has three remaining parameters, noise of the electronics, gas gain fluctuations, and the yield of the transition radiation photons. Noise of the electronics and gas gain fluctuations are tuned by using the energy deposit distributions of pion sample. These two parameters are tuned at each TRD layers at each momenta. Figure 4.20 shows the energy deposit distribution of pion and the simulation result at 4 GeV/c at the first layer of TRD. In the figure, the closed squares (blue) are real data and the smooth line (light blue) is simulation. The agreement on the energy deposit distribution on pion is very good.

The yield of the transition radiation photon is tuned at the first layer of TRDs at each momentum after the other parameters are fixed. Figure 4.21 shows the energy deposit distribution of electron and the simulation result at 4 GeV/c at the first layer of TRD. In this figure, the closed circles (red) are real data and the smooth line (pink) is simulation. The agreement on the energy deposit distribution on electron is also good.

Figure 4.22 shows the mean of the energy deposit of electron and pion as a function of drift time at 4 GeV/c. The left panel is for electron and the right panel is for pion. The contribution of TR photon is clearly seen at the end of drift time in case of electron. For the calculation of pion efficiency, the drift zone is divided into 6 regions by the drift time, as shown in Fig. 4.22. This process is almost same as the analysis of real data. The relationship between the drift time and the drift region is summarized at Table 4.5.

Since the avalanche process at the amplifier region is not simulated well, so that the drift

region 1 is not used for the calculation of pion efficiency. It will be safe to do this, since the absorption of the TR photon is not occurred at the drift region 1 or 2.

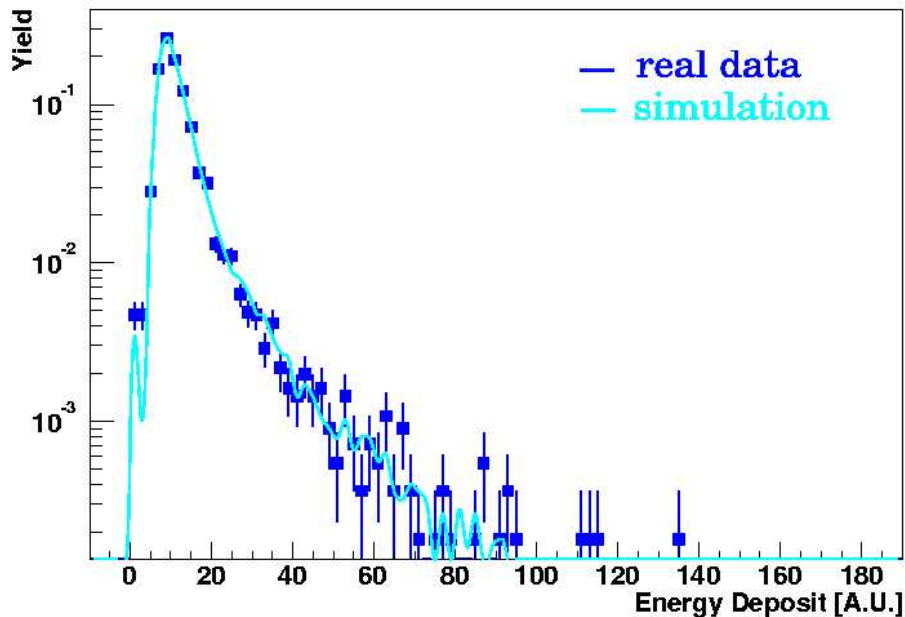


Figure 4.20: The energy deposit distribution of pion and the simulation result at 4 GeV/c at the first layer of TRD.

The energy deposit distributions of the real data and the simulation at the other momentum are shown in Figure 4.23. At the upper panel, momentum is 6 GeV/c, at the middle panel 8 GeV/c and the lower panel 10 GeV/c. The left panels are the distributions for pion and the right panels are these for electrons. In the figure, the closed circles (red) show real data of electron, the smooth lines (green) show the simulation of electron, the closed squares (blue) show real data of pion and the smooth lines (light blue) are the simulation of pion. At all momenta, the agreements on the energy deposit distribution on electron and pion are good.

Table 4.5: The relationship between the drift time and the drift region

drift region	1	2	3	4	5	6
drift time (μs)	0.2-0.6	0.6-1.0	1.0-1.4	1.4-1.8	1.8-2.2	2.2-2.6

4.4.2 The effect of material budget corresponding to FEE

In this section, the effect of knockout electrons on pion efficiency is studied by the simulation which is described in Section 4.4.1. Especially, the effect of increasing knockout electron due to

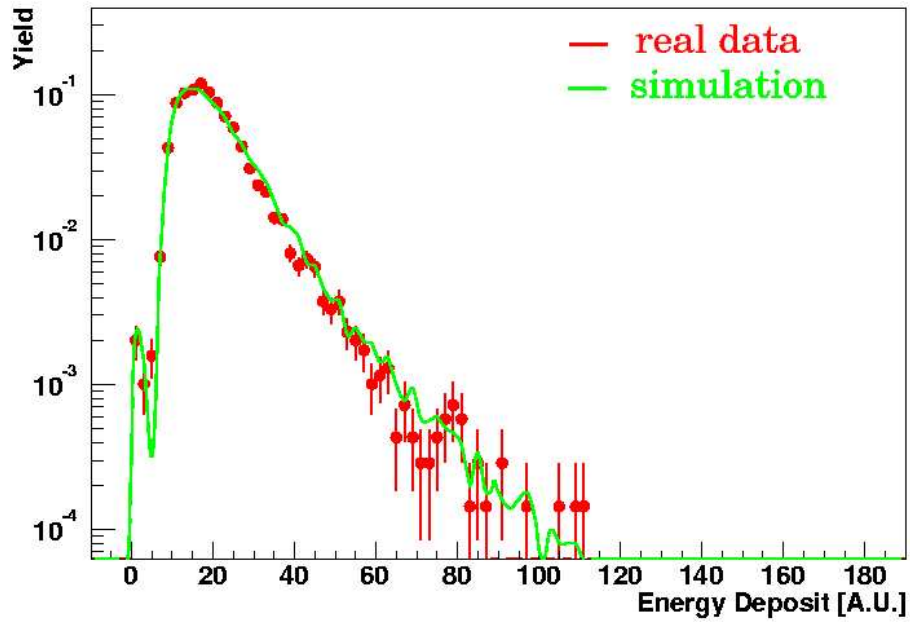


Figure 4.21: The energy deposit distribution of electron and the simulation result at 4 GeV/c at the first layer of TRD.

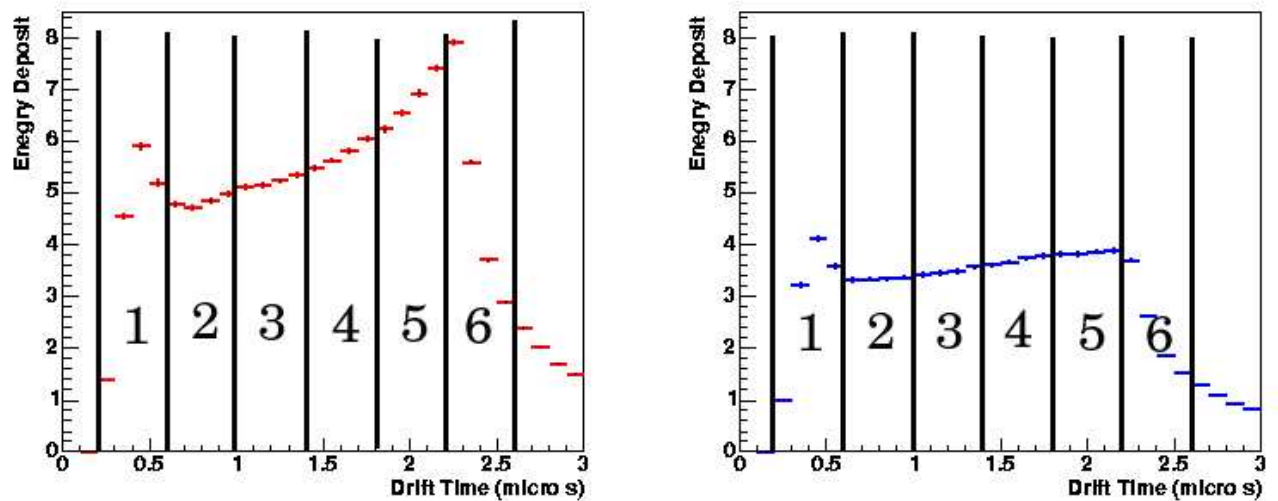


Figure 4.22: The mean of the energy deposit of electron and pion as a function of drift time at 4 GeV/c. The left panel is electron and the right panel is pion.

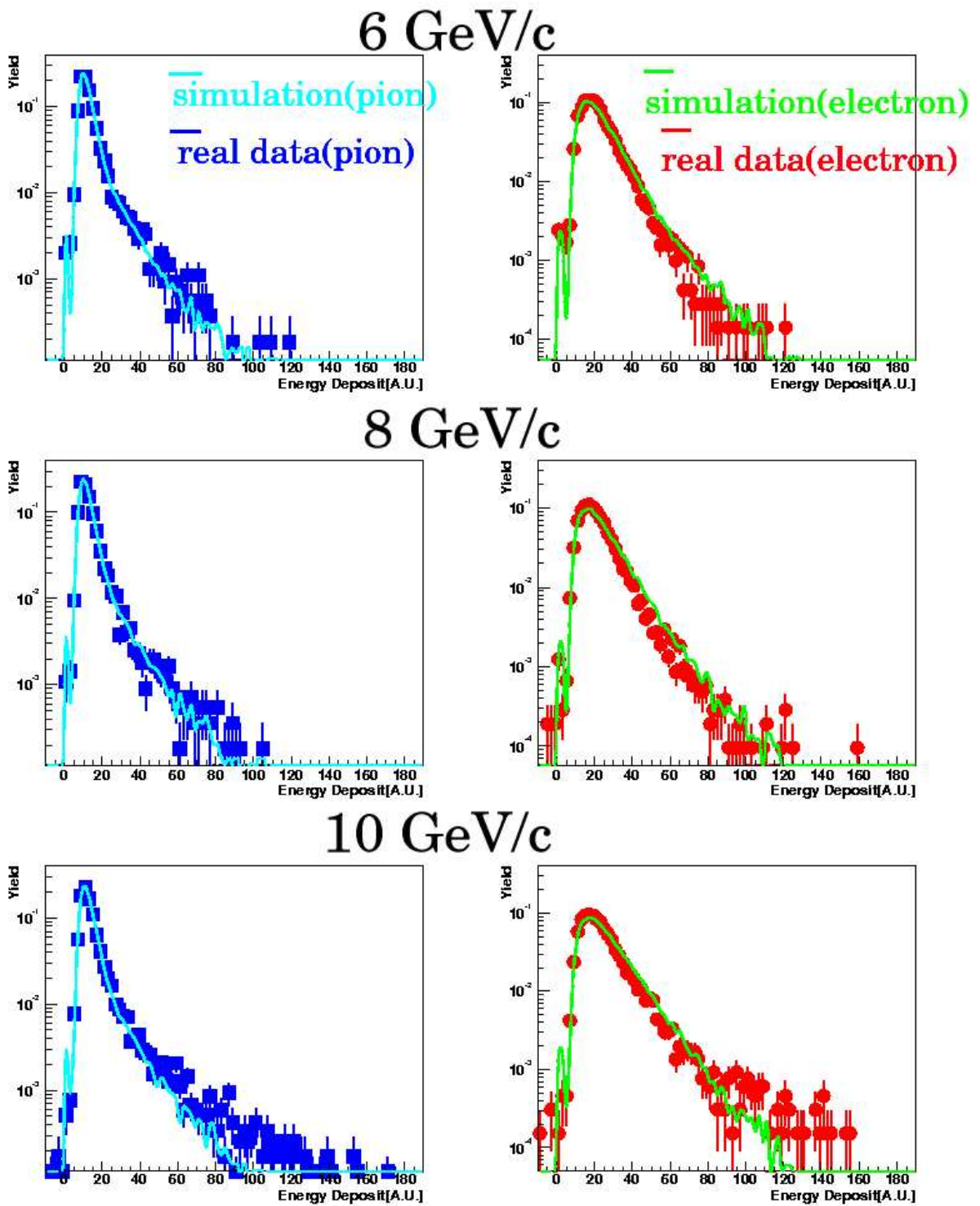


Figure 4.23: The energy deposit distributions of the real data and the simulation at the 6, 8 and 10 GeV/c at the first layer of TRDs.

material budget corresponding to FEE and the difference between the extrapolation of small prototype's result and the result of the real size TRD are studied.

For this purpose, the simulations are performed for the two cases; The one is with FEE and another is without FEE. The other conditions are the same. Figure 4.24 shows the event normalized energy spectrum of knockout electrons which arrived at the sixth layer of TRDs at 4 GeV/c in the case of pion. The closed circles (red) are in case of with FEE and the closed squares are in case of without FEE. The mean number of knockout electron per event is 0.079 with FEE and 0.034 without FEE. So the mean number of knockout electron per event differs more than factor 2 due to FEE.

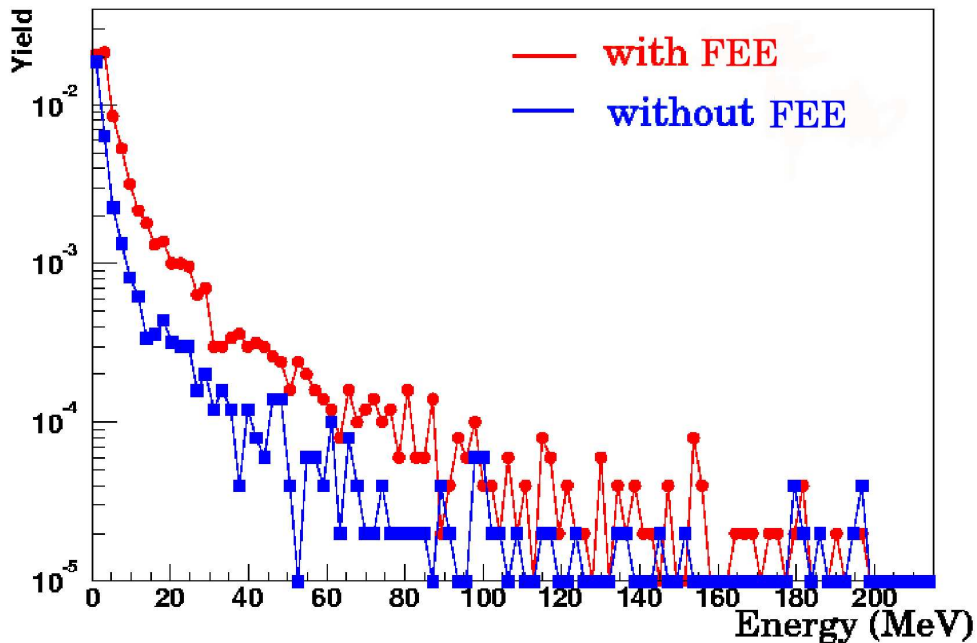


Figure 4.24: The event normalized energy spectrum of knockout electrons which arrived at the sixth layer of TRDs at 4 GeV/c in the case of pion.

Pion efficiency is calculated for both cases by bi-dimensional likelihood method, as described in Section 4.3.3. Figure 4.25 shows the pion efficiency of the simulation and real data as a function of the number of TRD layers used for analysis at 4 GeV/c. In this figure, the closed circles (red) show the result of real size TRD, the closed triangles (blue) show the result of small prototype. The reverse triangles (green) show the results from the simulation with FEE and the closed squares (black) show the results from the simulation without FEE. The difference of pion efficiency between the small prototype and the real size TRD at 4 TRD layers is about 0.5%, and the difference of pion efficiency between the simulation with FEE and without FEE is 0.3%. This two difference is comparable. The difference of pion efficiency between the small prototype and the real size TRD and that between the simulation with FEE and without FEE become large with the number of TRD layers.

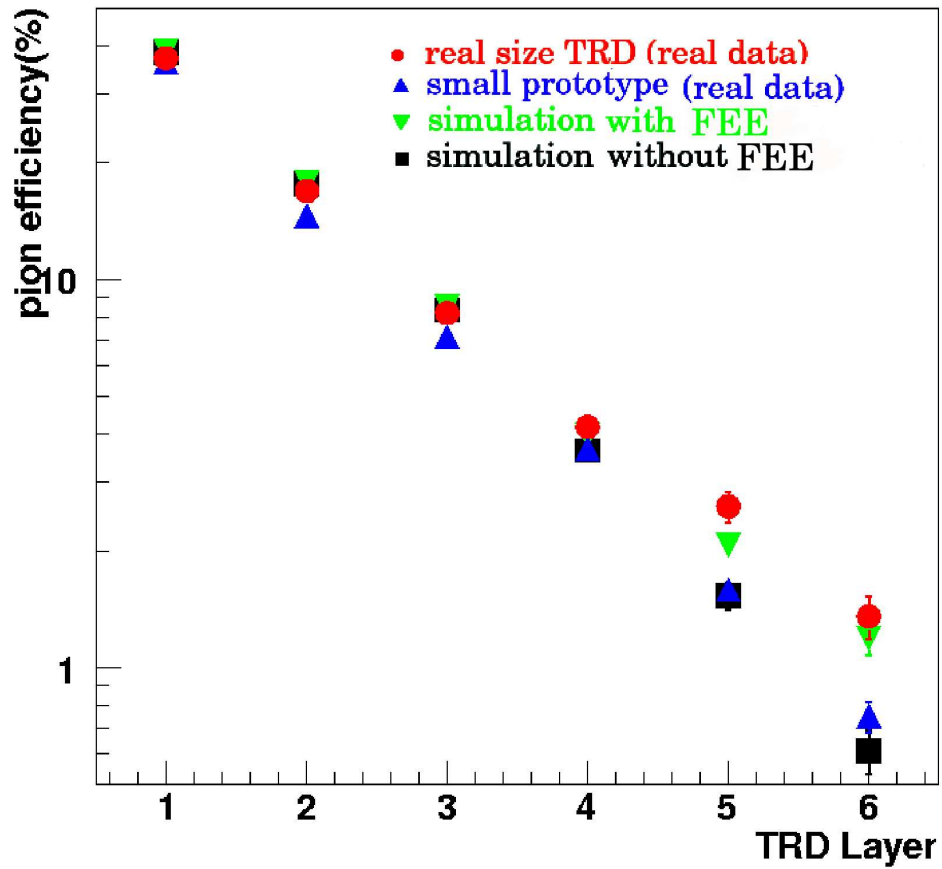


Figure 4.25: The pion efficiency of the simulation and real data as a function of the number of TRD layers used for analysis at 4 GeV/c. The simulations are two case, with FEE and without FEE. When the numbers of TRD layers are 5 and 6, the results of the small are the extrapolated values.

Figure 4.26 shows a ratio of the pion efficiency of the real size TRD to the small prototype and that of the pion efficiency of the simulation with FEE to the simulation without FEE as a function of the number of TRD layers. The closed squares (blue) is the ratio of the pion efficiency of the real size TRD to the small prototype, and the closed circles (red) is that of the pion efficiency of the simulation with FEE to the simulation without FEE. The ratio of the simulations almost agrees with the ratio of real data at each the number of TRD layers. So, the difference of the pion efficiency between the real size TRD and small prototype could be understood as the effect of knockout electrons due to larger material budget. Since the number of knockout electrons per event is a few % at sixth layer, the effect of knockout electrons becomes large when the pion efficiency is the same order.

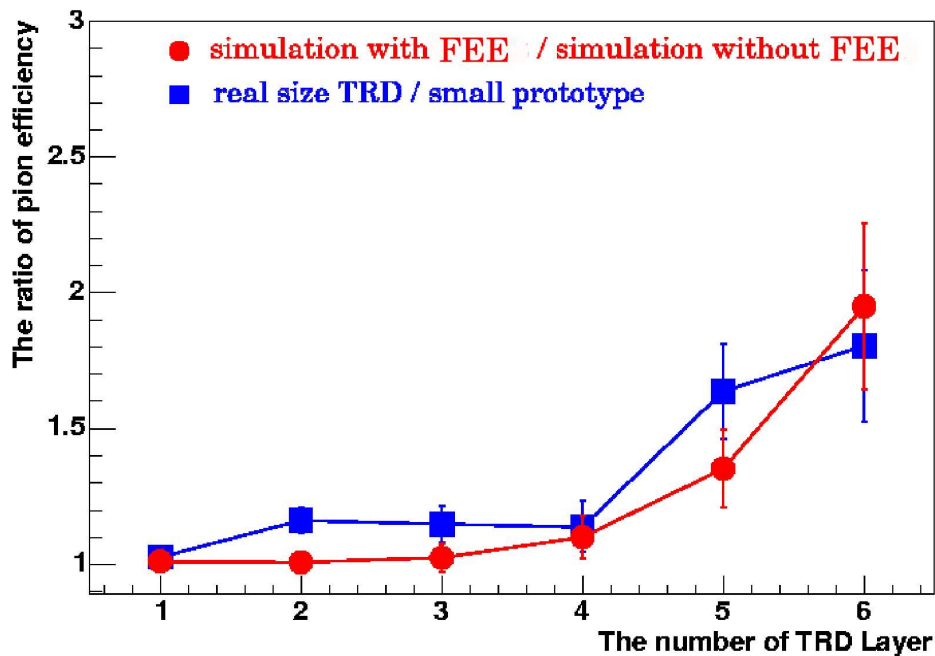


Figure 4.26: A ratio of the pion efficiency of real size TRD to small prototype and that of the pion efficiency of the simulation with MCMs to the simulation without FEE as a function of the number of TRD layers.

4.4.3 The effect of magnetic field

As described in Section 3.2.2 and in Section 2.1, the real size TRD was not operated under magnetic field, while ALICE TRD will be operated under 0.4 T magnetic field at the ALICE experiment.

Fig 4.24 shows that the energy of most of knockout electrons is below 20 MeV. So, the most of knockout electrons will have small the radius of curvature and go away from the parent track if TRDs are operated under magnetic field. In the case of operation under magnetic

field, the most of knockout electron will not reach the readout chamber. It is expected that under magnetic field the pion efficiency gets near the extrapolated value of the small prototype, because there are little correlation between the response of TRD layers due to the decreasing effect of knockout electrons.

For the effect of magnetic field on the pion efficiency, the simulation under 0.4 T magnetic field is done. This simulation is completely the same as the simulation with FEE which is done at Section 4.4.2 expect the existence of magnetic field. Figure 4.27 shows the event normalized energy spectrum of knockout electrons which arrived at the sixth layer of TRDs at 4 GeV/c in case of pion. The closed circles (red) are in case of operation at no field and the closed squares are in case of operation under magnetic field. The number of knockout electron per event is 0.079 in case of operation at no field and 0.023 in case of operation under magnetic field. A factor 3 decrease of the number knockout electron is seen due to the magnetic field.

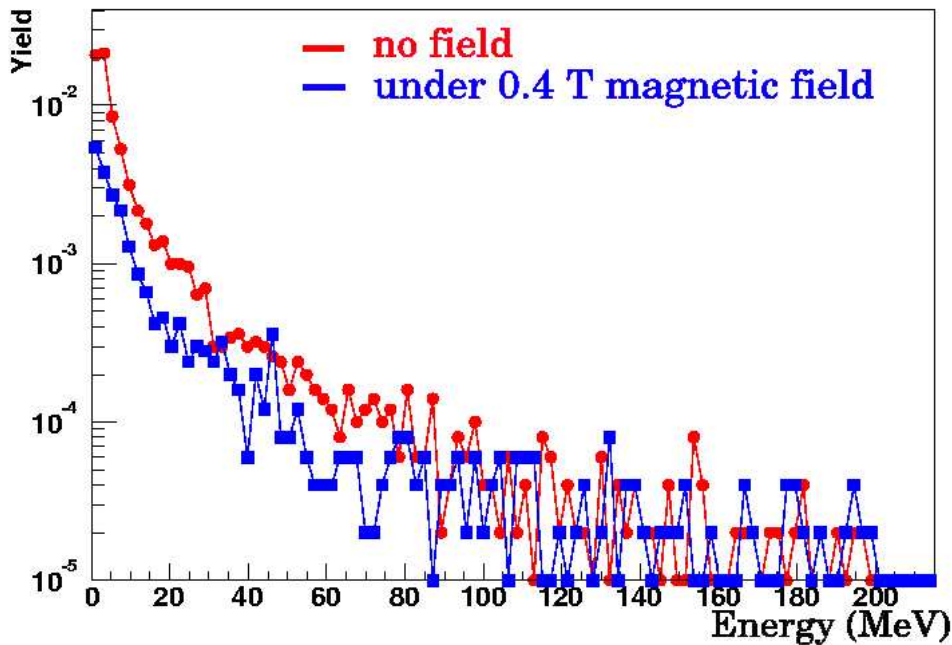


Figure 4.27: The event normalized energy spectrum of knockout electrons which arrived at the sixth layer of TRDs at 4 GeV/c in the case of pion.

The pion efficiency is also calculated for both case by bi-dimensional likelihood method, as described in Section 4.3.3. Figure 4.28 is the pion efficiency of the simulation and real data as a function of the number of TRD layers used for analysis at 4 GeV/c. In the figure, the closed circles (red) show the results of real size TRD, the closed triangles (blue) show the results of small prototype The closed reverse triangles (green) show the results from the simulation under no field and the closed squares (black) show the results from the simulation under the magnetic field.

The pion efficiency under the magnetic field gets near the extrapolated value of the small

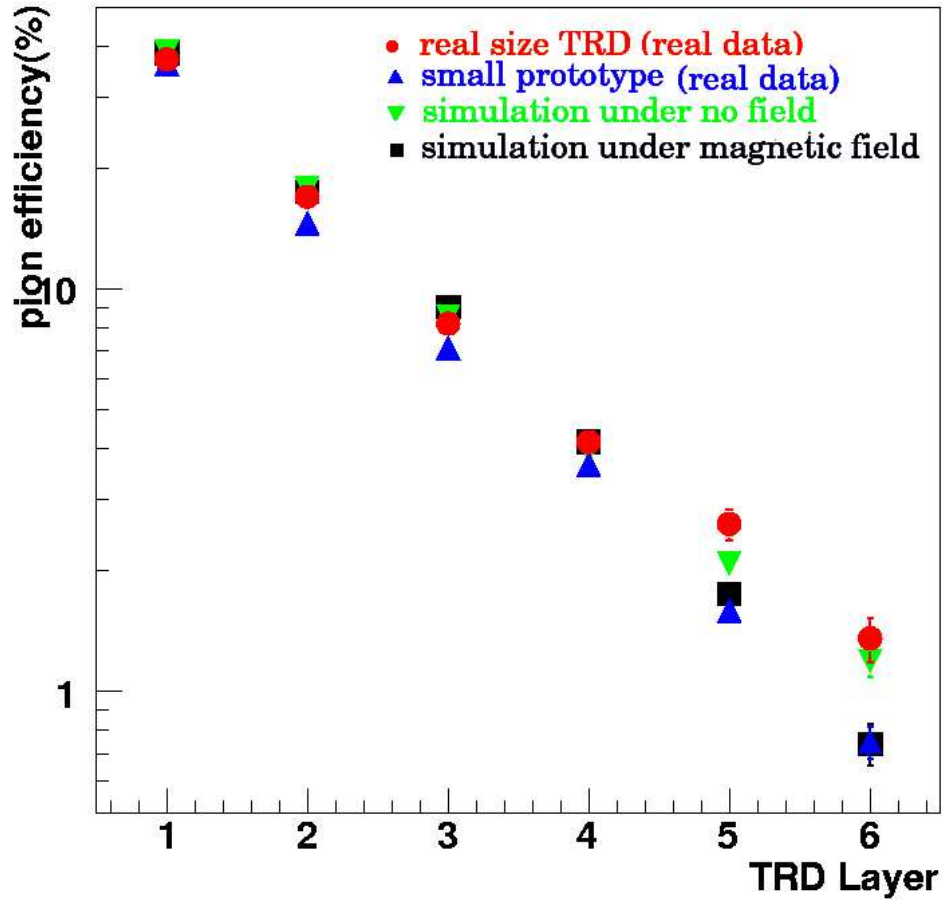


Figure 4.28: Pion efficiency of the simulation and real data as a function of the number of TRD layers used for analysis at 4 GeV/c. The simulations are two case, under no magnetic field and magnetic field. When the numbers of TRD layers are 5 and 6, the results of the small are the extrapolated values.

prototype result. Using 6 TRD layer, the pion efficiency of the simulation becomes 0.8% under the magnetic field. This result is within the requirement of ALICE TRD, which the pion efficiency is below 1% above 3 GeV/c at 90% electron efficiency. So, real size TRD will provide enough the capability of electron identification at the ALICE experiment.

Figure 4.29 shows the pion efficiency of the simulation under the magnetic field as a function of momentum, with the result of real size TRD and small prototype. The closed squares (red) show the results of the real size TRD, the closed circles (blue) show the extrapolated value of the result of the small prototype and the closed triangles (green) show the results of the simulation under the magnetic field. These results are summarized in Table 4.6

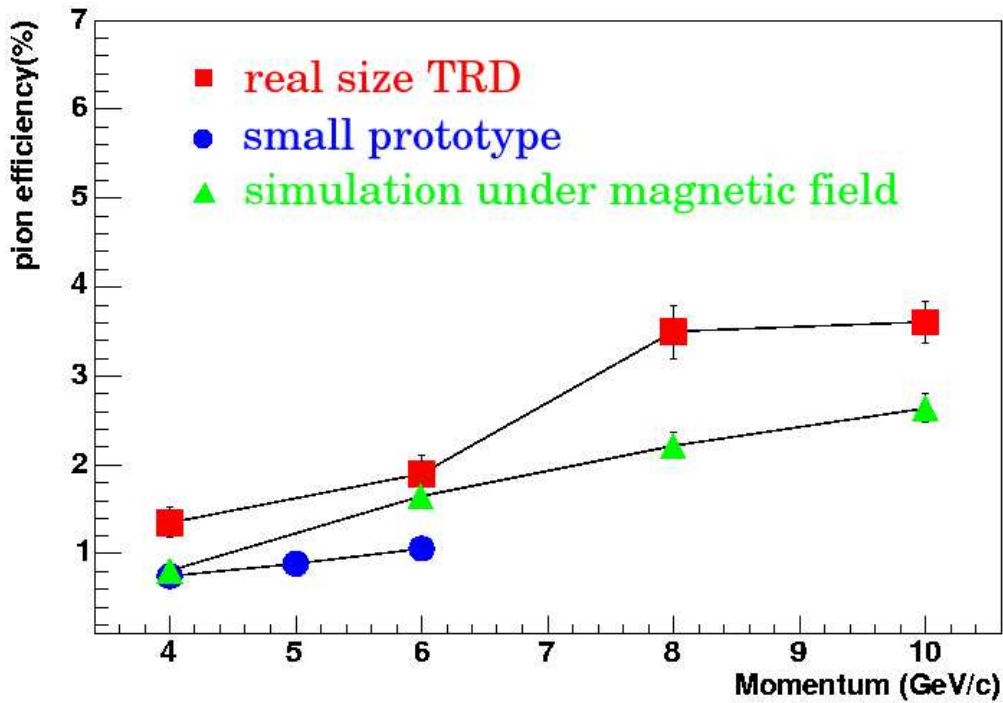


Figure 4.29: Pion efficiency of the simulation and real data as a function of momentum. The simulation is under magnetic field.

Table 4.6: The pion efficiency of real size TRD and the simulation under magnetic field.

Momenta (GeV/c)	4	6	8	10
pion efficiency (one-dimensional likelihood)	1.96	2.93	4.45	3.82
pion efficiency (bi-dimensional likelihood)	1.35	1.90	3.50	3.61
pion efficiency (the simulation under magnetic field)	0.80	1.64	2.20	2.63

Chapter 5

Conclusion

ALICE is an experiment at LHC optimized for heavy ion collision at $\sqrt{s_{NN}} = 5.5$ TeV. The physics goal of ALICE is to study the property of hot QGP, its dynamical evolution, hadronization, and evolution of hadronic state.

TRDs will provide capability of charged particle tracking and electron identification at ALICE. Specially, TRD is the main detector for electron identification at high momentum region (above 3 GeV/c).

After several test beam experiments with the small prototype TRD, the test beam experiment with real size TRD was performed in the fall of 2002 at CERN. In this thesis, the capability of electron identification of real size TRD is studied.

Using bi-dimensional likelihood method, the pion efficiency of real size TRD obtained 1.35% at 4 GeV/c. This result is near the requirement of ALICE TRD, which is the pion efficiency below 1% at electron efficiency 90% above electron transverse momenta above 3 GeV/c. The extrapolated value of the small prototype result is 0.75%. It is considered that the difference between real size TRD and the extrapolated value of the small prototype is caused by the correlation of the response of TRD layer due to knockout electrons.

For the confirmation of the above consideration, simulation study is done. By decreasing material budget corresponding to MCMS, the pion efficiency of the simulation gets near the extrapolated value of the small prototype, while the pion efficiency of the simulation with MCM is almost same as the result of real size TRD.

At the ALICE experiment, TRD will be operated under 0.4 T magnetic field. Under magnetic field, knockout electron will go away from the parent track. Consequently, better pion efficiency is expected under magnetic field. The pion efficiency of the simulation under magnetic field becomes 0.80% at 4 GeV/c. This result satisfies the requirement of ALICE TRD. And at the higher momentum, pion efficiency is slightly above 1%. The real size TRD will provide enough the capability of electron identification at the ALICE experiment.

Acknowledgment

I'm grateful to Prof. H. Hamagaki, first of all. His appropriate advice and rich knowledge helped me to study the electron identification capability of the ALICE TRD.

I thank Dr. Anton Andronic and thank the members of the ALICE TRD Collaborate for their help in the data analysis and a great deal of valuable advice. I appreciate Dr. K. Ozawa for many comments and advice on data analysis and this thesis. I thank to Mr. T. Gunji and Mr. S. Saito for there help through the test experiment and data analsis. I thank to Mr. S. Oda for many kind comments for this theis.

Finally, I wish to express my gratitude to my parents and my friends.

Bibliography

- [1] D. Gross and F. Wilczek, Phys. Rev. Lett. **30** (1973) 1343.
- [2] J. C. Collins and M. J. Perry, Phys. Rev. Lett. **34** (1975) 1353.
- [3] E. V. Shuryak, Phys. Rep. **61** (1980) 71.
- [4] S. Gottlieb *et al.*, Phys. Rev. D. **55** (1997) 6852.
- [5] K. Adcox *et al.*, Nucl. Phys. A. **757** (2005) 184.
- [6] B. Muller, Rep. Prog. Phys. **58** (1995) 611.
- [7] ALICE Collaboration, Technical Proposal, CERN/LHCC/97-71.
- [8] ALICE Collaboration, A Transition Radiation Detector, Technical Proposal, Addendum 1, CERN/LHCC/96-32.
- [9] ALICE Collaboration, A Transition Radiation Detector, Technical Design Report, CERN/LHCC/2001-21.
- [10] T. Matsui and H. Satz, Phys. Lett. **B178**, 416 (1986).
- [11] S. Digal, P. Petreky and H. Satz, Phys. Rev. **D64**, 094015 (2001).
- [12] P. Braun-Munzinger and J. Stachel, Phys. Lett. **B490**, 1966 (2000).
- [13] R. Thews and J. Rafelski, Nucl. Phys. **A698**, 575 (2002).
- [14] V.L. Ginzburg and I.M. Frank, Zh. Exsp. Theor. Fiz. **16** (1946) 15.
- [15] L. G. Christophorou *et al.*, Nucl. Instr. Meth. **171** (1980) 491.
- [16] O. Busch *et al.*, Nucl. Instr. Meth. **A525**,(2004) 508.
- [17] C. Adler *et al.*, Nucl. Instr. Meth. **A540**,(2005) 140.
- [18] C. Adler *et al.*, Nucl. Instr. Meth. **A552**,(2005) 364.
- [19] A. Andronic, Nucl. Instr. Meth. **A522** (2004) 40.
- [20] A. Andronic *et al.*, Nucl. Instr. Meth. **A525** (2004) 447.

- [21] A. Andronic *et al.*, Nucl. Instr. Meth. **A498** (2003) 143.
- [22] I. Rusanov and J. Stachel, GSI Annual Report 2004, p 354.
- [23] ALICE TRD Collaboration, GSI Annual Report 2004, p 355.
- [24] <http://www.kip.uni-heidelberg.de/ti/ACEXBoard/>
- [25] <http://aldwww.cern.ch/>
- [26] W. Blum and L. Rolandi, Particle Detection with Drift Chambers, Springer-Verlag, 1994.
- [27] GEANT4 Collaboration, CERN/LHCC 98-44 and
<http://wwwinfo.cern.ch/asd/geant/geant4.html>
- [28] <http://AliSoft.cern.ch/offline/>